SCALABLE OPTIMIZATION METHOD FOR GENERATOR SCHEDULING UNDER UNCERTAINTY

by

EDWARD ARTHUR QUARM JNR.

Dissertation

Submitted in partial fulfillment of the requirements
for the degree of Doctor of Philosophy at
The University of Texas at Arlington
December, 2021

Arlington, Texas

Supervising Committee:

Dr. Ramtin Madani, Supervising Professor
Dr. Ali Davoudi
Dr. Farhad Kamangar
Dr. Ioannis Schizas
Dr. David Levine
Dr. Wei-Jen Lee, Graduate Advisor

ABSTRACT

SCALABLE OPTIMIZATION METHOD FOR GENERATOR SCHEDULING UNDER UNCERTAINTY

EDWARD ARTHUR QUARM JNR., Ph.D.

The University of Texas at Arlington, 2021

Supervising Professor: Dr. Ramtin Madani

Scalable optimization methods for power system operation has been subject of research over the last 60 years. State-of-the-art methods in this research area is yet to yield the scalability desired by system operators for practical operation of electric grids. This article-based dissertation makes three significant contributions. A scalable computational method is developed to tackle a mixed-integer problem commonly referred to as Stochastic Security-Constrained Unit Commitment (SSCUC), the output of which will be beneficial to Independent System Operators to manage electric grids. Secondly, an improved model for time-progressive contingencies in security-constrained optimization problems is presented. This modeling approach is more realistic representation of contingency modeling as compared to what exists in literature. Finally, uncertainty from pulsed load transients in microgrids is tackled in the presence of energy storage units.

In the first paper, a detailed SSCUC problem is considered that suffers from complexities posed by the presence of binary variables, uncertainty of renewable energy and security constraints. The second paper deals with extra challenges time-progressive contingencies such as hurricanes and wildfires pose to the Security-Constrained Optimal Power

Flow (SCOPF) problem. The third paper deals with the MG scheduling problem in the presence of uncertainty introduced by transient load demand.

ACKNOWLEDGEMENTS

I would like to express my deepest appreciation to my supervising professor Dr. Ramtin Madani for his endless support, and also for his invaluable advice during the course of my doctoral studies. I wish to thank my committee members Dr. Ali Davoudi, Dr. Farhad Kamangar, Dr. Ioannis Schizas and Dr. David Levine for providing me insightful suggestions and valuable feedback.

I am forever grateful to my dad and mom, without them I won't be the person I am today. To my wife, you are my rock; thank you so much for being there for me throughout this stage of my life.

December, 2021

TABLE OF CONTENTS

ABSTRACT ii

ACKNOWLEDGEMENTS v

LIST OF ILLUSTRATIONS ix

LIST OF TABLES xi

Chapter Page

1. INTRODUCTION 1

1.1 Research Overview 1

1.2 Summary of Publications 1

2. SCALABLE SECURITY-CONSTRAINED UNIT COMMITMENT UNDER UNCERTAINTY VIA CONE PROGRAMMING RELAXATION 4

2.1 INTRODUCTION 7

2.1.1 Notation 10

2.2 UNIT COMMITMENT PROBLEM 10

2.2.1 Problem Formulation 11

2.2.2 Objective function 12

2.2.3 Constraints 14

2.3 CONVEXIFICATION OF SCUC PROBLEM 18

2.3.1 Lifted objective 18

2.3.2 LP and perspective relaxations 20

2.3.3 SDP relaxation 21

2.4 FEASIBLE POINT RECOVERY 23

2.5 EXPERIMENTS 25

2.5.1 Data . . . 26
2.5.2 Evaluation of Lower Bound . . . 30
2.5.3 Solution Quality . . . 30
2.5.4 Hourly Profile . . . 32
2.5.5 Network Congestion . . . 34
2.6 CONCLUSIONS . . . 35
3. PROACTIVE POSTURING OF LARGE POWER GRID FOR MITIGATING HURRICANE IMPACTS . . . 37
3.1 INTRODUCTION . . . 40
3.1.1 Notations . . . 42
3.2 MODELING HURRICANE'S IMPACT ON GRID AND THE OPTIMIZATION PROBLEM FORMULATION . . . 42
3.2.1 Hurricane Contingency Description . . . 43
3.2.2 Multi-period Proactive SCOPF Problem Formulation . . . 43
3.2.3 Multi-Step Cascaded Optimization Problem considering Hurricane Progression . . . 45
3.3 NUMERICAL RESULTS . . . 46
3.3.1 Operation Cost . . . 47
3.3.2 Proactive Mitigation Measure . . . 48
3.4 CONCLUSIONS . . . 48
4. MICROGRID SCHEDULING WITH UNCERTAINTY IN TRANSIENT LOAD 50
4.1 INTRODUCTION . . . 53
4.1.1 Notations . . . 56
4.2 MG SCHEDULING PROBLEM . . . 56
4.2.1 Multi-scenario Load demand Profile . . . 57
4.2.2 Problem Formulation . . . 58

4.2.3 Objective function 59
4.2.4 Constraints 60
4.3 CONVEXIFICATION OF MG SCHEDULING PROBLEM 63
4.3.1 Lifted objective 63
4.3.2 LP and perspective relaxations 65
4.3.3 SDP relaxation 67
4.4 FEASIBLE POINT RECOVERY 69
4.5 EXPERIMENTS 71
4.5.1 Evaluation of Lower Bound 73
4.5.2 Utilizing Energy Storage Units to Compensate Variability in Load Profile 74
4.6 CONCLUSIONS 76
5. GENERAL CONCLUSIONS 77
5.1 Conclusions 78
5.2 Future Research Direction 79
REFERENCES 80
BIOGRAPHICAL STATEMENT 91

LIST OF ILLUSTRATIONS

Figure Page

2.1 Distribution of Binary variables for PEGASE 1354 (Experiment 14) in 24-hour horizon scheduling 31

2.2 Distribution of Binary variables for PEGASE 2869 (Experiment 17) in 24-hour horizon scheduling 32

2.3 New-England 39-bus (Experiment 1) 24-hr profile showing generator output and line flows. First from top: Gen. 2 base case and post-contingency power output showing transition probabilities across 3 scenarios. Second from top: Gen. 5 base case and post-contingency power output across 3 scenarios. Third from top: Line 38 basecase and post-contingency power flows across 3 scenarios. 34

2.4 Directed graph of New England 39-bus Pre and Post-contingencies 35

3.1 An illustration of multi-step cascaded optimization considering hurricane progression. 46

3.2 Line MVA flows on line # 77 before and after applying proactive mitigation to penalize the flow on selected lines in the hurricane path 49

4.1 Load demand profiles. First from top: group 1 - Base loads. Second from top: group 2 - Peak loads. Third from top - Transient loads. 58

4.2 IEEE 14-bus Microgrid test system; showing ESUs placement in Experiment 5 . . 74

4.3 Impact of Energy Storage Units on load variability at 200ms time scales. First from top: DG and ESU power output in the presence of Group 1 (base loads). Second from top: DG and ESU power output in the presence of Group 1 & 2 (base + Peak loads). Third from top: DG and ESU power output in the presence of Group 1, 2 & 3 (base + peak + transient loads. Forth from top: ESU charge and discharge power output in scenario # 3. 75

LIST OF TABLES

Table		Page
2.1	Experiments for 24-hour horizon scheduling of benchmark systems	31
2.2	The performance of SDP relaxation algorithm for 24-hour horizon scheduling of benchmark systems (4 realizations in each benchmark system)	32
2.3	Generator data for New England 39-bus benchmark system (Experiment 1)	33
2.4	Binary commitment decisions for New England 39-bus benchmark system (Experiment 1)	33
3.1	Contingency Data and Operation Cost	47
4.1	Generator Parameters	73
4.2	Comparative performance of SDP relaxation algorithm to off-the-shelf solvers and selected convex relaxations	74

CHAPTER 1

INTRODUCTION

1.1 Research Overview

At the center of operating the US electric grids are Independent System Operators (ISOs) whose aim is to facilitate the real-time and day-ahead operation. ISOs have to deal with a changing conditions under which the grid operates. These changes are commonly referred to as uncertainties. For example, renewable energy sources such as wind and solar power cause variability in power generation while low-frequency high impact events such as hurricanes, floods and other natural disasters affect system reliability.

This dissertation examines the complexity of tackling challenging day-ahead scheduling problems in cases where large-scale UC is combined with security constraints, contingency events and uncertain wind scenarios. Secondly, electricity security is investigated in the presence of hurricane contingencies. This research work was part of an internship opportunity at Pacific Northwest National Laboratory in summer 2021. The results of this dissertation can be adopted by ISOs for daily operation of the US electric grid, national laboratories to conduct studies on the large-scale grids in US and the broad research community for further advancement.

1.2 Summary of Publications

This dissertation is presented in an article-based format and includes three research papers; 1 published journal paper, 1 published conference paper and 1 manuscript under preparation. Chapter 2 presents the paper titled, "Scalable Security-Constrained Unit Commitment Under Uncertainty via Cone Programming Relaxation", which was published in IEEE

Transactions on Power Systems Journal in 2021. This paper is co-authored and includes the following author: Dr. Ramtin Madani. As the primary author, I was responsible for formulating the problem and performing experiments. Dr. Madani supervised the research work by providing feedback on research directions, reviewing and editing the manuscript.

This paper proposed a scalable method to deal with computationally challenging SCUC problems. The method was tested extensively on IEEE and PEGASE benchmark systems to establish its relative performance against two widely used solvers, CPLEX and GUROBI together with the state-of-the-art perspective and linear programming. We show that the proposed semidefinite programming relaxation consistently finds near-globally optimal solutions for each benchmark system under uncertain wind scenarios and with an extensive list of contingencies with up to 12,240 binary variables and 1,830,560 continuous variables.

Chapter 3 presents a conference paper titled, "Proactive Posturing of Large Power Grid for Mitigating Hurricane Impacts ",which is to appear in 2022 IEEE PES Conference on Innovative Smart Grid Technologies (ISGT 2022). This paper is co-authored by: Xiaoyuan Fan, Marcelo Elizondo and Ramtin Madani. As the primary author, I was responsible for formulating the problem and performing experiments. Dr. Xiaoyuan Fan supervised the research work; Dr. Marcelo Elizondo co-supervised research work and Dr. Ramtin Madani contributed to providing feedback on problem formulation and final version of manuscript.

This paper aims to develop interactive cross-domain data analytics based on hurricane modeling, power system optimization and model-based simulations. The temporal relations among individual steps (groups of time period) within historical hurricane event have been explored and transformed into explicit optimization constraints, and further incorporated into SCOPF problem to identify proactive posturing of power system elements. Variations of the operation cost among different hurricane steps (contingency batches) in-

dicates the applicability of such optimization formulation, and the improvement in targeted credible line contingencies shows promising improvements by such proactive dispatch.

Chapter 4 presents a manuscript under preparation for publication titled, "Microgrid Scheduling with Uncertainty in Transient Load". This paper is co-authored by: Dr. Ramtin Madani. As the primary author, I was responsible for problem formulation and performing experiments. Dr. Ramtin Madani supervised the research work by providing feedback on research directions, reviewing and editing the manuscript.

In this paper, we presented the Microgrid (MG) scheduling problem under load demand uncertainty. MGs by design have smaller network size and suffer from inadequate reserve margins as compared to main grids. As a result, highly variable load like transient load demand can negatively affect reliability. To tackle this challenge in the MG scheduling problem, we make use of semidefinite programming relaxation which is capable of finding feasible solutions within provable distance from global optimality. It is shown that the proposed SDP relaxation finds optimal solutions to the scheduling problem without need to adopt scenario reduction techniques when mixed-integer programming solvers are utilized. Furthermore, we demonstrated that the problem of load variability can be greatly reduced with the help of Energy Storage Units (ESUs) when scheduled in tandem with Distributed Generators (DGs). The analysis performed can serve as a guide to MG operators in finding the approximate size of ESUs needed to achieve a desired load profile in a scheduling problem with the objective of minimizing operation cost.

Finally, Chapter 5 presents general conclusions and directions for future research work.

CHAPTER 2

SCALABLE SECURITY-CONSTRAINED UNIT COMMITMENT UNDER UNCERTAINTY VIA CONE PROGRAMMING RELAXATION

Scalable Security-Constrained Unit Commitment Under Uncertainty via Cone Programming Relaxation[1]

E. Quarm and R. Madani, "Scalable Security-Constrained Unit Commitment Under Uncertainty via Cone Programming Relaxation," in IEEE Trans. on Power Systems, vol. 36, no. 5, pp. 4733-4744, Sept. 2021, doi: 10.1109/TPWRS.2021.3062203.

Scalable Security-Constrained Unit Commitment under Uncertainty via Cone Programming Relaxation

Edward Quarm Jnr. and Ramtin Madani

The authors are with the Department of Electrical Engineering, University of Texas at Arlington (email: edwardarthur.quarmjnr@uta.edu, ramtin.madani@uta.edu).

Abstract — This paper is concerned with the problem of Security-Constrained Unit Commitment (SCUC) which is a long-standing challenge in power system engineering faced by system operators and utility companies on a daily basis. We consider a detailed variant of this problem that suffers from complexities posed by the presence of binary variables, the uncertainty of renewable sources and security constraints. A convex relaxation is formulated which is capable of finding feasible solutions within a provable distance from global optimality. We demonstrate the performance of this approach on detailed and challenging instances of SCUC with IEEE and PEGASE benchmark cases from The proposed approach is able to handle over 12,000 binary variables and 2 million continuous variables with significant improvement in solution quality over commonly-used off-the-shelf solvers and other methods of convex relaxation.

Keywords — Power generation scheduling, Power system security, Optimization methods.

2.1 INTRODUCTION

Unit commitment (UC) is the problem of determining the schedule and level of contributions by generators in a power grid to meet forecasted demand for electricity as economically as possible. The efficiency of wholesale power markets is highly dependent on solution methods for UC. Efficient algorithms based on high-fidelity power grid models can alleviate a variety of problems such as uplift payments, underfunded transmission rights and occasional disputes between market participants [1, 2]. Several variants of UC have been studied in the literature to address considerations such as contingency constraints and to mitigate the uncertainty of demand and renewable sources. Network components are prone to various sources of failure. Hence, contingency planning is central to reliable functioning of power grids. To ensure immunity to the outage of individual grid components, it is common-practice to impose a comprehensive list of constraints, accounting for pre-determined contingencies. This problem is regarded as Security-Constrained Unit Commitment (SCUC). Due to the ever increasing integration of renewable energy sources, several papers have considered stochastic formulations of SCUC to mitigate the risks associated with grid uncertainty. In this paper, we propose a computational method for SCUC under the uncertainty of renewable sources.

The presence of binary variables pose a major challenge in solving large-scale unit commitment problems. Therefore, a variety of methods have been developed for UC since the late 1960s. Among early attempts were rudimentary methods such as exhaustive enumeration and priority list [3–7] that are only applicable to small instances of UC. In the 1960s and 70s a number of Dynamic Programming (DP) methods were proposed for UC in [8–10], without success on large-scale problems due to curse of dimensionality. To this date, Lagrangian Relaxation (LR) has remained one of the successful methods to approach UC [11–13]. LR works by decomposing UC problems into a master problem and subproblems that are solved iteratively until an optimal solution is found. The success of LR

is due to its reliance on a lower complexity dual formulation as opposed to the high dimensional primal UC problem which is tackled by other methods. Recent papers employ benders decomposition for separating the UC into master and subproblems to be solved using augmented LR or combined with DP and Genetic Algorithm (GA) [14–16] to achieve reasonable computational speed, though not fast enough for practical applications.

With the increase in computer memory and processing power Mixed-Integer Programming (MIP) methods such as Branch and Bound (B&B) have gained popularity as solution approaches to UC [17, 18]. Recently, MIP solvers such as CPLEX and GUROBI have become very popular and widely used to solve UC problems for commercial applications [1]. However, a main disadvantage of B&B is the rapid growth of search trees with the number of binary variables [19]. The success of MIP solvers in tackling stochastic SCUC problems depends on the tightness and compactness of formulation, number of binary variables, number of wind scenarios, number of contingencies and binding transmission line constraints [20–22]. In order to improve the efficiency and solution quality of B&B searches, the creators of CPLEX; IBM have offered improvements such as heuristics, node presolve and cutting planes [23]. Despite these improvements, a number of papers have reported that the computational burden on off-the-shelf MIP solvers increases when applied to large-scale SCUC problems as solvers either exceed the time-limit or CPU memory limit [20–22]. Many papers have also offered partial convex hull characterizations of UC feasible sets [24–27] to improve efficiency of B&B. The paper [28] offers a critical review of the common-practice of implementing linear programming (LP) relaxation as a reliable approach to UC.

Recently, more sophisticated convex relaxations such as Semidefinite Programming (SDP) and Second-Order Cone Programming (SOCP) have been used for solving different variants of UC [29, 30]. In [29], it is shown that perspective relaxation can significantly improve the performance of MIP search for UC. The paper [30] applies SDP relaxation

to SCUC with AC network constraints. In [31] a strengthened SDP relaxation is proposed, which offers improved performance using the Reformulation Linearization Technique (RLT). The paper [32] employs SOCP to find globally optimal solutions to UC with AC network constraints. Due to the computational complexity of UC, solutions obtained from any polynomial-solvable relaxation may not be feasible for the original non-convex UC problem. To address this issue, the paper [33] proposes a sequential penalization method for UC to obtain near-globally optimal solutions.

This paper examines the complexity of tackling challenging day-ahead scheduling problems in cases where large-scale UC is combined with security constraints, contingency events and uncertain wind scenarios. We adopted a stochastic approach proposed in [34]. The base case and contingency states are tied together by generator ramp limits. In addition, generator re-dispatches are treated as recourse actions to contingencies. This stochastic approach to modeling system security is preferred to other modeling approaches because it allows for cost of each state to be weighted by its probability of occurrence.

In this paper, we leverage the power of SDP relaxation to alleviate the burden of branch-and-bound search for detailed and large-scale SCUC problems. While off-the-shelf SDP relaxation produces a lower bound on the optimal objective, it is computationally prohibitive thus not scalable [35, 36]. Hence, in this work, we are forging a low-complexity conic relaxation that is capable of solving large-scale SCUC. This effort is aligned with the recent body of research devoted to scalable variants of semidefinite programming [37]. In lieu of computationally demanding constraints, we employ low-order SDP constraints to determine binary variables. So as to strengthen the relaxation, valid inequalities are introduced from the multiplication of constraints through the Reformulation-Linearization Technique (RLT). To address cases for which the proposed relaxation is not exact, we propose a heuristic approach to infer near-globally optimal points from the outcome of convex relaxation. The proposed approach is tested on modified IEEE and PEGASE benchmark

systems with realizations of uncertain wind scenarios and N-1 contingencies. The largest benchmark system considered includes 12,240 binary decision variables and 1,830,560 continuous variables. The performance of the proposed convex relaxation is compared with off-the-shelf solvers such as CPLEX and GUROBI and other methods of relaxation like perspective and LP relaxations.

The remainder of this paper is organized as follows. In Section 2.2.1, we formulate the SCUC problem under uncertainty. This non-convex problem is convexified by means of convex surrogates in Section 2.3. Next, a scalable convex relaxation is proposed in Section 2.3 to tackle SCUC in polynomial time. Section 2.4 proposes a heuristic approach to infer near-globally optimal points from the outcome of convex relaxation. Extensive experiments are conducted in Section 2.5 on IEEE and PEGASE benchmark systems. Section 2.6 concludes the paper.

2.1.1 Notation

Throughout this paper, matrices, vectors and scalars are represented by boldface uppercase, boldface lowercase and italic lowercase letters, respectively. $|\cdot|$ represents the absolute value of a scalar or the cardinality of a set. The symbol $(\cdot)^\top$ represents the transpose operator. The notation real$\{\cdot\}$ represents the real part of a scalar or a matrix. Given a matrix $\boldsymbol{A}$, the notation $\boldsymbol{A}_{jk}$ refers to its $(j,k)^{th}$ element. $\boldsymbol{A} \succeq 0$ means that $\boldsymbol{A}$ is symmetric and positive semidefinite.

2.2 UNIT COMMITMENT PROBLEM

This work considers a secure unit commitment problem under wind generation uncertainty. As mentioned in the introduction, security constraints are modeled using a stochastic approach proposed in [34]. Contingencies in the network are modeled by specifying outages to units or lines. Locational reserve requirements are endogenously determined as a func-

tion of the set of included credible contingencies, which is in stark contrast to deterministic approach where zonal reserve requirements are predefined by system operators and employed in various UC studies [14]. Pre-defined or fixed reserve requirements are not used in this study, conversely we make use of generator ramp rate modeled after [38]. Also, we define a power contract variable which represents reference dispatch value from which dispatch deviations are defined.

Uncertainty in wind generation is modeled as scenarios with continuous probability distributions, such that each scenario represents a different forecast of wind. Furthermore, a transition probability matrix is used to describe the transitions from a limited set of base scenarios in one period to a limited set of base scenarios in the next period. Experimental data on generator and wind parameters including ramp rate for IEEE and PEGASE benchmark systems are specified in Section 2.5.

2.2.1 Problem Formulation

The goal of unit commitment is to schedule the generation of electricity within a time horizon $\mathcal{T} = \{1, 2, \ldots, |\mathcal{T}|\}$. For every $t \in \mathcal{T}$, let $\mathcal{S}_t$ represent the set of all possible uncertainty scenarios for renewable sources at time t. Additionally, let $\mathcal{G}_t$ represent the set of all generating units that are available at time $t \in \mathcal{T}$. For every, $t \in \mathcal{T}$ and $s \in \mathcal{S}_t$, define $\mathcal{C}_{ts}$ as the set of all contingency cases with $0 \in \mathcal{C}_{ts}$ representing the base case (normal operation). Lastly, $\mathcal{G}_{tsc} \subseteq \mathcal{G}_t$ is defined as the set of all generating units that are available at time $t \in \mathcal{T}$, scenario $s \in \mathcal{S}_t$ and contingency $c \in \mathcal{C}_{ts}$, such that

$$\mathcal{G}_t = \cup_{s \in \mathcal{S}_t} \cup_{c \in \mathcal{C}_{ts}} \mathcal{G}_{tsc}.$$

Consider a power system with $\mathcal{V}$ as the set of buses, and $\mathcal{E}_{tc} \subseteq \mathcal{V} \times \mathcal{V}$ as the set of branches at time $t \in \mathcal{T}$ and contingency $c \in \cup_{s \in \mathcal{S}_t} \mathcal{C}_{ts}$.

Motivated by [34], we formulate SCUC using the following list of decision variables:

$$\{x_{tg} \in \{0,1\}\}_{t\in\mathcal{T},\, g\in\mathcal{G}_t}, \qquad \{p^{\text{contract}}_{tg},\ r^{+}_{tg},\ r^{-}_{tg},\ w^{+}_{tg},\ w^{-}_{tg} \in \mathbb{R}\}_{t\in\mathcal{T},\, g\in\mathcal{G}_t}$$

$$\{p_{tgsc}\}_{t\in\mathcal{T},\, g\in\mathcal{G}_t,\, s\in\mathcal{S}_t,\, c\in\mathcal{C}_{ts}}, \qquad \left\{\boldsymbol{\theta}_{tsc} \in \mathbb{R}^{|\mathcal{V}|}\right\}_{t\in\mathcal{T},\, s\in\mathcal{S}_t,\, c\in\mathcal{C}_{ts}}.$$

Each x_{tg} is a binary variable indicating the on/off status of unit $g \in \mathcal{G}_t$ at time $t \in \mathcal{T}$ and p^{contract}_{tg} is its contract active power quantity. Variables (r^{+}_{tg}, r^{-}_{tg}) are upward and downward contingency reserve quantities, and (w^{+}_{tg}, w^{-}_{tg}) represent upward and downward load-following ramping reserve quantities, respectively. If $g \notin \mathcal{G}_t$, then

$$x_{tg} = p^{\text{contract}}_{tg} = r^{+}_{tg} = r^{-}_{tg} = w^{+}_{tg} = w^{-}_{tg} = 0.$$

Each variable p_{tgsc} denotes the active power injection at time $t \in \mathcal{T}$ by generator $g \in \mathcal{G}_t$, in scenario $s \in \mathcal{S}_t$ and contingency $c \in \mathcal{C}_{ts}$. Lastly, $\boldsymbol{\theta}_{tsc} \in \mathbb{R}^{|\mathcal{V}|}$ represents the vector of nodal phase angles at time $t \in \mathcal{T}$, scenario $s \in \mathcal{S}_t$ and contingency $c \in \mathcal{C}_{ts}$.

2.2.2 Objective function

We consider a holistic objective accounting for the expected value of the total cost throughout the time horizon $\mathcal{T}$, and across the set of all scenarios and contingencies. This objective is made up of the expected base case and post-contingency generation costs, ramping "wear and tear" costs, load-following ramp reserve and contingency reserve costs, as well as the

generator start-up, shutdown and fixed costs. This objective function can be cast with respect to the following three expressions:

$$\sum_{t\in\mathcal{T}} \gamma_t \sum_{g\in\mathcal{G}_t} \sigma_{tg}^{(1)}(x_{tg}, r_{tg}^{+}, r_{tg}^{-}, w_{tg}^{+}, w_{tg}^{-}) \tag{2.1a}$$

$$\sum_{t\in\mathcal{T}} \sum_{s\in\mathcal{S}_t} \sum_{c\in\mathcal{C}_{ts}} \psi_{tsc} \sum_{g\in\mathcal{G}_{tsc}} \sigma_{tg}^{(2)}(p_{tgsc}, p_{tg}^{\text{contract}}) \tag{2.1b}$$

$$\sum_{t\in\mathcal{T}} \gamma_t \sum_{s_1\in\mathcal{S}_{t-1}} \sum_{s_2\in\mathcal{S}_t} \phi_{ts_1s_2} \sum_{g\in\mathcal{G}_{ts_20}} \sigma_{g}^{(3)}(p_{tgs_20}, p_{(t-1)gs_10}) \tag{2.1c}$$

In the first line of the objective (2.1a), the cost function $\sigma_{tg}^{(1)}$is defined as

$$\sigma_{tg}^{(1)}(x_{tg}, r_{tg}^{+}, r_{tg}^{-}, w_{tg}^{+}, w_{tg}^{-}) \triangleq \zeta_{tg}\ x_{tg} \tag{2.2a}$$

$$+\ \zeta_{tg}^{\uparrow}\ (1 - x_{(t-1)g})x_{tg} \tag{2.2b}$$

$$+\ \zeta_{tg}^{\downarrow}\ x_{(t-1)g}(1 - x_{tg}) \tag{2.2c}$$

$$+\ (\eta_{tg}^{+}\ r_{tg}^{+} + \eta_{tg}^{-}\ r_{tg}^{-}) \tag{2.2d}$$

$$+\ (\mu_{tg}^{+}\ w_{tg}^{+} + \mu_{tg}^{-}\ w_{tg}^{-}) \tag{2.2e}$$

with the expressions (2.2a), (2.2b) and (2.2c) corresponding to generator fixed, startup and shutdown costs, respectively; while (2.2d) and (2.2e) account for the cost of contingency and load-following ramping reserves, respectively. The start-up and shutdown costs $\zeta_{tg}^{\uparrow}$ and $\zeta_{tg}^{\downarrow}$ incur with every time slot at which the unit changes status. The fixed production cost ζ_{tg} is enforced if the unit is active. The coefficients η_{tg}^{+} and η_{tg}^{-} are the costs incurred when reserves are purchased from a generating unit in the event of a contingency. The coefficients μ_{tg}^{+} and μ_{tg}^{-} are the costs incurred due to variations of active power between two consecutive time slots in which the unit g is committed. These costs are weighted

by γ_t, which is the probability of transitioning to period t without branching off from the central base case path to a contingency.

In the second line (2.1b), the function $\sigma_{tg}^{(2)}(\cdot,\cdot)$ is defined as

$$\sigma_{tg}^{(2)}(p_{tgsc}, p_{tg}^{\text{contract}}) \triangleq \alpha_{tg}^{\text{sqr}}\ p_{tgsc}^2 + \alpha_{tg}^{\text{lin}}\ p_{tgsc} + \tag{2.3a}$$

$$\frac{\beta_{tg}^+ + \beta_{tg}^-}{2}\,|\,p_{tgsc} - p_{tg}^{\text{contract}}| + \frac{\beta_{tg}^+ - \beta_{tg}^-}{2}(p_{tgsc} - p_{tg}^{\text{contract}}) \tag{2.3b}$$

including the quadratic expression (2.3a) with nonnegative quadratic and linear coefficients α_{tg}^{sqr} and α_{tg}^{lin}, and the term (2.3b) for assigning costs to deviations from contract values with nonnegative coefficients β_{tg}^+ and β_{tg}^-. These costs are weighted by the probability of contingency ψ_{tsc}.

Finally, we have the third term (2.1c) representing a quadratic load-following ramp "wear and tear" cost

$$\sigma_g^{(3)}(p_{tgs_20}, p_{(t-1)gs_10}) \triangleq \kappa_g \times (p_{tgs_20} - p_{(t-1)gs_10})^2 \tag{2.4}$$

weighted by γ_t, the nonnegative coefficients κ_g, and $\phi_{ts_1s_2}$ which is the probability of transitioning to scenario s_2 in period t provided that scenario s_1 was realized in period $t-1$.

2.2.3 Constraints

We apply the following constraints which can be separated into five main categories:

2.2.3.1 Integrality constraints

For every $t \in \mathcal{T}$ and $g \in \mathcal{G}_t$, the binary requirements are:

$$x_{tg} \in \{0, 1\} \tag{2.5}$$

These constraints are the main sources of complexity in SCUC. We will relax the integrality constraints (2.5) and implicitly impose them via proxy conic and linear inequalities.

2.2.3.2 Unit capacity constraints

For every $t \in \mathcal{T}$ and $g \in \mathcal{G}_t$, the unit capacity constraints consist of:

$$\underline{p}_g \, x_{tg} \leq p_{tgsc} \leq \bar{p}_g \, x_{tg} \qquad \forall s \in \mathcal{S}_t, \; \forall c \in \mathcal{C}_{ts} \tag{2.6}$$

Constraint (2.6) ensures that when unit $g \in \mathcal{G}_t$ is committed during the interval t, then its active power injections lies within the pre-specified limits $\underline{p}_{tgsc}$ and $\bar{p}_{tgsc}$.

2.2.3.3 Minimum up/down time constraints

For every $t \in \mathcal{T}$ and $g \in \mathcal{G}_t$, the Minimum up/down time constraints are:

$$x_{tg} \geq x_{\tau g} - x_{(\tau-1)g} \qquad \forall \tau \in \{t - m_g^{\uparrow} + 1, \ldots, t\} \tag{2.7a}$$

$$1 - x_{tg} \geq x_{(\tau-1)g} - x_{\tau g} \qquad \forall \tau \in \{t - m_g^{\downarrow} + 1, \ldots, t\} \tag{2.7b}$$

where $m_g^{\uparrow}$ and $m_g^{\downarrow}$ denote the minimum up and down time limits of generator t, respectively.

2.2.3.4 Ramp constraints

For every $t \in \mathcal{T}$ and $g \in \mathcal{G}_t$, the generator ramp constraints consist of:

$$0 \leq w^{+}_{tg} \leq \bar{w}_{tg}, \tag{2.8a}$$

$$0 \leq w^{-}_{tg} \leq \underline{w}_{tg}, \tag{2.8b}$$

$$p_{tgs_2 0} - p_{(t-1)gs_1 0} \leq w^{+}_{(t-1)g}, \qquad \forall s_1 \in \mathcal{S}_{t-1},\ \forall s_2 \in \mathcal{S}_t \tag{2.8c}$$

$$p_{(t-1)gs_1 0} - p_{tgs_2 0} \leq w^{-}_{(t-1)g}, \qquad \forall s_1 \in \mathcal{S}_{t-1},\ \forall s_2 \in \mathcal{S}_t \tag{2.8d}$$

Constraints (2.8a) – (2.8b) impose the limits $\bar{w}_{tg}$ and $\underline{w}_{tg}$ on the upward and downward load-following reserve quantities of generator t, respectively. Constraints (2.8c) – (2.8d) limit changes in active power injection between two consecutive time slots during which the unit t is committed.

2.2.3.5 Post-contingency reserve constraints

For every $t \in \mathcal{T}$ and $g \in \mathcal{G}_t$, the post-contingency reserve constraints are:

$$0 \leq r^{+}_{tg} \leq \bar{r}_{tg}, \tag{2.9a}$$

$$0 \leq r^{-}_{tg} \leq \underline{r}_{tg}, \tag{2.9b}$$

$$p_{tgsc} - p^{\text{contract}}_{tg} \leq r^{+}_{tg}, \qquad \forall s \in \mathcal{S}_t,\ \forall c \in \mathcal{C}_{ts} \tag{2.9c}$$

$$p^{\text{contract}}_{tg} - p_{tgsc} \leq r^{-}_{tg}, \qquad \forall s \in \mathcal{S}_t,\ \forall c \in \mathcal{C}_{ts} \tag{2.9d}$$

$$-\underline{\Delta}_g \leq p_{tgsc} - p_{tgs0} \leq \bar{\Delta}_g, \qquad \forall s \in \mathcal{S}_t,\ \forall c \in \mathcal{C}_{ts} \tag{2.9e}$$

Constraints (2.9a) – (2.9b) impose the upward/downward reserve capacity limits $\bar{r}_{tg}$ and $\underline{r}_{tg}$ on post-contingency dispatch quantities, respectively. Deviations from active power contract quantities are limited by constraints (2.9c) – (2.9d). Additionally, the constraint

(2.9e) enforces the physical ramp limits $\underline{\Delta}_g$ and $\bar{\Delta}_g$ on downward and upward transitions from base to post-contigency cases.

2.2.3.6 DC network constraints

The DC modeling is employed to describe the flow of power throughout the network. To this end, let $\boldsymbol{B}$ denote the the imaginary part of the network bus admittance matrix and for each $t \in \mathcal{T}$ and $c \in \cup_{s\in\mathcal{S}_t}\mathcal{C}_{ts}$, let $\vec{\boldsymbol{B}}_{tc} \in \mathbb{R}^{|\mathcal{E}_{tc}|\times|\mathcal{V}|}$ and $\boldsymbol{B}_{tc} \in \mathbb{R}^{|\mathcal{V}|\times|\mathcal{V}|}$ represent the corresponding susceptance matrices. Additionally, define $\boldsymbol{C}_{tsc} \in \{0,1\}^{|\mathcal{G}_{tsc}|\times|\mathcal{V}|}$ as the incidence matrix whose (j,k) element is equal to 1, if and only if the unit g belongs to the bus k. For every $t \in \mathcal{T}$, the DC network constraints can be cast as

$$\boldsymbol{d}_{tc} + \boldsymbol{B}_{tc}\,\boldsymbol{\theta}_{tsc} = \boldsymbol{C}_{tsc}^{\top}\,\boldsymbol{p}_{tsc}, \qquad \forall s \in \mathcal{S}_t,\ \forall c \in \mathcal{C}_{ts} \tag{2.10a}$$

$$|\vec{\boldsymbol{B}}_{tc}\,\boldsymbol{\theta}_{tsc} + \boldsymbol{f}_{tc}^{\text{shift}}| \leq \boldsymbol{f}_{tc}^{\max} \qquad \forall s \in \mathcal{S}_t,\ \forall c \in \mathcal{C}_{ts} \tag{2.10b}$$

where

$$\boldsymbol{p}_{tsc} \triangleq [p_{t1sc},\ p_{t2sc},\ \ldots,\ p_{t|\mathcal{G}_{tsc}|sc}]^{\top} \tag{2.11}$$

Constraint (2.10a) imposes power balance equation in which $\boldsymbol{d}_{tc} \in \mathbb{R}^{|\mathcal{V}|}$ represents nodal demand and the vector $\boldsymbol{B}_{tc}\theta_{tsc} \in \mathbb{R}^{|\mathcal{V}|}$ contains approximate values for active power exchanges between each vertex and the rest of the network. Additionally, constraint (2.10b) restricts the flow of power by the vector of line thermal limits $\boldsymbol{f}_{tc}^{\max} \in \mathbb{R}^{|\mathcal{E}_{tc}|}$, where $\boldsymbol{f}_{tc}^{\text{shift}}$ accounts for the effect of transformers and phase shifters.

Given the above three-part expression in (2.1) and constraints in (2.5) – (2.10), the Stochastic SCUC problem can be formulated as the optimization:

$$\begin{aligned}
&\text{minimize} && \text{(2.1a)+(2.1b)+(2.1c)} && && \text{(2.12a)}\\
&\text{subject to} && \text{(2.5)} - \text{(2.9)} && \forall t \in \mathcal{T},\ \ \forall g \in \mathcal{G}_t && \text{(2.12b)}\\
& && \text{(2.10)} && \forall t \in \mathcal{T} && \text{(2.12c)}
\end{aligned}$$

with respect to variables $\{x_{tg}\}$, $\{p_{tgsc}\}$, $\{p_{tg}^{\text{contract}}\}$, $\{r_{tg}^{+}\}$, $\{r_{tg}^{-}\}$, $\{w_{tg}^{+}\}$, and $\{w_{tg}^{-}\}$.

2.3 CONVEXIFICATION OF SCUC PROBLEM

In this section, we construct convex relaxations in order to efficiently tackle the SCUC problem (2.12). We employ conic relaxations combined with a set of valid inequalities which lead to a computationally-tractable convex formulation. To this end, we transition to a lifted space by introducing additional auxiliary variables each accounting for a quadratic monomial. We then formulate a SOCP relaxation based on the "perspective relaxation" in [39]. Finally, a strong SDP relaxation is formulated using additional variables and valid inequalities.

2.3.1 Lifted objective

To formulate convex relaxations we first lift the objective function (2.1) into a higher-dimensional space in which it is piecewise linear. This is done by introducing the variables

$$\big\{u_{tg}\big\}_{t\in\mathcal{T},\, g\in\mathcal{G}_t},\quad \big\{h_{tgs_1s_2}\big\}_{t\in\mathcal{T},\, g\in\mathcal{G}_t,\, s_1\in\mathcal{S}_{t-1},\, s_2\in\mathcal{S}_t},\quad \big\{o_{tgsc}\big\}_{t\in\mathcal{T},\, g\in\mathcal{G}_t,\, s\in\mathcal{S}_t,\, c\in\mathcal{C}_{ts}}$$

representing the products

$$\{x_{(t-1)g}\, x_{tg}\}, \quad \{p_{(t-1)gs_10} \times p_{tgs_20}\}, \quad \{p^2_{tgsc}\} \tag{2.13}$$

respectively. Consider the following lifted objective function components:

$$\sum_{t\in\mathcal{T}} \gamma_t \sum_{g\in\mathcal{G}_t} \bar{\sigma}^{(1)}_{tg}(x_{tg}, u_{tg}, r^+_{tg}, r^-_{tg}, w^+_{tg}, w^-_{tg}) \tag{2.14a}$$

$$\sum_{t\in\mathcal{T}} \sum_{s\in\mathcal{S}_t} \sum_{c\in\mathcal{C}_{ts}} \psi_{tsc} \sum_{g\in\mathcal{G}_{tsc}} \bar{\sigma}^{(2)}_{tg}(p_{tgsc}, o_{tgsc}, p^{\text{contract}}_{tg}) \tag{2.14b}$$

$$\sum_{t\in\mathcal{T}} \gamma_t \sum_{s_1\in\mathcal{S}_{t-1}} \sum_{s_2\in\mathcal{S}_t} \phi_{ts_1s_2} \sum_{g\in\mathcal{G}_{ts_20}} \bar{\sigma}^{(3)}_{g}(o_{tgs_20}, o_{(t-1)gs_10}, h_{tgs_2s_1}) \tag{2.14c}$$

where for each $t \in \mathcal{T}$ and $g \in \mathcal{G}_t$

$$\bar{\sigma}^{(1)}_{tg}(x_{tg}, u_{tg}, r^+_{tg}, r^-_{tg}, w^+_{tg}, w^-_{tg}) \triangleq \zeta_{tg}\; x_{tg} \tag{2.15a}$$

$$+ \zeta^{\uparrow}_{tg}\; (x_{tg} - u_{tg}) \tag{2.15b}$$

$$+ \zeta^{\downarrow}_{tg}\; (x_{(t-1)g} - u_{tg}) \tag{2.15c}$$

$$+ (\eta^+_{tg}\; r^+_{tg} + \eta^-_{tg}\; r^-_{tg}) \tag{2.15d}$$

$$+ (\mu^+_{tg}\; w^+_{tg} + \mu^-_{tg}\; w^-_{tg}) \tag{2.15e}$$

encapsulates the lifted startup and shutdown costs and

$$\bar{\sigma}^{(2)}_{tg}(p_{tgsc}, o_{tgsc}, p^{\text{contract}}_{tg}) \triangleq \alpha^{\text{sqr}}_{tg}\; o_{tgsc} + \alpha^{\text{lin}}_{tg}\; p_{tgsc} + \tag{2.16a}$$

$$\frac{\beta^+_{tg}+\beta^-_{tg}}{2}\,|\,p_{tgsc} - p^{\text{contract}}_{tg}| + \frac{\beta^+_{tg}-\beta^-_{tg}}{2}(p_{tgsc} - p^{\text{contract}}_{tg}). \tag{2.16b}$$

represents the lifted quadratic cost function. Additionally, for each $g \in \mathcal{G}$,

$$\bar{\sigma}_g^{(3)}(o_{tgs_20}, o_{(t-1)gs_10}, h_{tgs_1s_2}) \triangleq \kappa_g \times (o_{tgs_20} + o_{(t-1)gs_10} - 2h_{tgs_1s_2}) \tag{2.17}$$

is the lifted "wear and tear" cost.

2.3.2 LP and perspective relaxations

For every $t \in \mathcal{T}$ and $g \in \mathcal{G}_t$, the relation between the auxiliary variables $\{u_{tg}\}$ and their corresponding monomials can be enforced using the following valid inequalities:

$$\max\{0,\ x_{(t-1)g} + x_{tg} - 1\} \leq u_{tg} \leq \min\{x_{(t-1)g}, x_{tg}\} \tag{2.18}$$

The role of (2.18) is to ensure that the lifted costs (2.14a) is equivalent to the original costs (2.1a). Through simple enumeration of the set $(x_{g(t-1)}, x_{gt}) \in \{0,1\}^2$, it can be observed that

$$\text{(2.5)} \wedge \text{(2.18)} \quad \Rightarrow \quad u_{tg} = x_{tg} x_{(t-1)g}$$

for every $t \in \mathcal{T}$ and $g \in \mathcal{G}_t$.

Lifting the first part of the objective and the transformation of $x_{gt} \in \{0,1\}$ to $0 \leq x_{tg} \leq 1$, results in the following LP relaxation of SCUC [40–42]:

minimize	(2.14a)+(2.1b)+(2.1c)		(2.19a)
subject to	$0 \leq x_{tg} \leq 1$	$\forall t \in \mathcal{T},\ \forall g \in \mathcal{G}_t$	(2.19b)
	(2.6) – (2.9), (2.18)	$\forall t \in \mathcal{T},\ \forall g \in \mathcal{G}_t$	(2.19c)
	(2.10)	$\forall t \in \mathcal{T}$	(2.19d)

As shown in [39], the performance of this approach can be significantly improved by lifting (2.1b) to (2.14b), and relaxing $o_{tgsc} = p_{tgsc}^2$ to the SOCP and McCormick constraint

$$o_{tgsc}\, x_{tg} \geq p_{tgsc}^2, \quad o_{tgsc} \geq 0 \qquad \forall s \in \mathcal{S}_t,\ \forall c \in \mathcal{C}_{ts} \tag{2.20a}$$

$$o_{tgsc} + \underline{p}_g\, \bar{p}_g\, x_{tg} \leq (\underline{p}_g + \bar{p}_g) p_{tgsc} \qquad \forall s \in \mathcal{S}_t,\ \forall c \in \mathcal{C}_{ts} \tag{2.20b}$$

which results in the following perspective relaxation:

$$\text{minimize} \qquad \text{(2.14a)+(2.14b)+(2.1c)} \tag{2.21a}$$

$$\text{subject to} \qquad 0 \leq x_{tg} \leq 1 \qquad \forall t \in \mathcal{T},\ \forall g \in \mathcal{G}_t \tag{2.21b}$$

$$\text{(2.6)} - \text{(2.9), (2.18), (2.20)} \qquad \forall t \in \mathcal{T},\ \forall g \in \mathcal{G}_t \tag{2.21c}$$

$$\text{(2.10)} \qquad \forall t \in \mathcal{T} \tag{2.21d}$$

In the remainder of this section, we will construct an SDP relaxation as an alternative to (2.21).

2.3.3 SDP relaxation

To forge a stronger relaxation, consider the new variables

$$\{z_{tgs}\}_{t \in \mathcal{T},\, g \in \mathcal{G}_t,\, s \in \mathcal{S}_t}, \qquad \{y_{tgs}\}_{t \in \mathcal{T},\, g \in \mathcal{G}_t,\, s \in \mathcal{S}_t}$$

$$\begin{bmatrix} x_{(t-1)g} & * & * & * & * \\ u_{tg} & x_{tg} & * & * & * \\ u_{tg} & u_{tg} & u_{tg} & * & * \\ p_{(t-1)gs_10} & z_{tgs_1} & z_{tgs_1} & o_{(t-1)gs_10} & * \\ y_{tgs_1} & p_{tgs_20} & y_{tgs_1} & h_{tgs_1s_2} & o_{tgs_20} \end{bmatrix} \succeq 0 \qquad \forall s_1 \in \mathcal{S}_{t-1},\ \forall s_2 \in \mathcal{S}_t \tag{2.22a}$$

$$\underline{p}_g \left(p_{tgs_10} + p_{tgs_20}\right) \ \leq \ h_{tgs_1s_2} + \underline{p}_g^2\, u_{tg} \qquad \forall s_1 \in \mathcal{S}_{t-1},\ \forall s_2 \in \mathcal{S}_t \tag{2.22b}$$

$$\bar{p}_g \left(p_{tgs_10} + p_{tgs_20}\right) \ \leq \ h_{tgs_1s_2} + \bar{p}_g^2\, u_{tg} \qquad \forall s_1 \in \mathcal{S}_{t-1},\ \forall s_2 \in \mathcal{S}_t \tag{2.22c}$$

$$h_{tgs_1s_2} + \underline{p}_g \bar{p}_g\, u_{tg} \ \leq \ \bar{p}_g\, y_{tgs_1} + \underline{p}_g\, z_{tgs_1} \qquad \forall s_1 \in \mathcal{S}_{t-1},\ \forall s_2 \in \mathcal{S}_t \tag{2.22d}$$

$$h_{tgs_1s_2} + \underline{p}_g \bar{p}_g\, u_{tg} \ \leq \ \underline{p}_g\, y_{tgs_1} + \bar{p}_g\, z_{tgs_1} \qquad \forall s_1 \in \mathcal{S}_{t-1},\ \forall s_2 \in \mathcal{S}_t \tag{2.22e}$$

$$\underline{p}_g\, u_{tg} \ \leq \ y_{tgs_1} \ \leq \ \bar{p}_g\, u_{tg} \qquad \forall s \in \mathcal{S}_t \tag{2.22f}$$

$$\underline{p}_g\, u_{tg} \ \leq \ z_{tgs_1} \ \leq \ \bar{p}_g\, u_{tg} \qquad \forall s \in \mathcal{S}_t \tag{2.22g}$$

$$\bar{p}_g \left(u_{tg} - x_{tg}\right) \ \leq \ y_{tgs_1} - p_{tgs0} \ \leq \ \underline{p}_g \left(u_{tg} - x_{tg}\right) \qquad \forall s \in \mathcal{S}_t \tag{2.22h}$$

$$\bar{p}_g \left(u_{tg} - x_{(t-1)g}\right) \ \leq \ z_{tgs_1} - p_{(t-1)gs0} \ \leq \ \underline{p}_g \left(u_{tg} - x_{(t-1)g}\right) \qquad \forall s \in \mathcal{S}_t \tag{2.22i}$$

representing monomials $\{p_{(t-1)gs0}x_{tg}\}$ and $\{p_{tgs0}x_{(t-1)g}\}$, respectively. In place of (2.19b), we impose a collection of conic and linear inequalities (2.22), resulting in the following SDP relaxation of SCUC:

$$\begin{aligned}
&\text{minimize} && \text{(2.14a)+(2.14b)+(2.14c)} && && \text{(2.23a)}\\
&\text{subject to} && \text{(2.22)} && \forall t \in \mathcal{T},\ \forall g \in \mathcal{G}_t && \text{(2.23b)}\\
& && \text{(2.6)}-\text{(2.9), (2.18), (2.20)} && \forall t \in \mathcal{T},\ \forall g \in \mathcal{G}_t && \text{(2.23c)}\\
& && \text{(2.10)} && \forall t \in \mathcal{T} && \text{(2.23d)}
\end{aligned}$$

The matrix inequality (2.22a) is a surrogate for:

$$\begin{bmatrix} x_{(t-1)g} & * & * & * & * \\ u_{tg} & x_{tg} & * & * & * \\ u_{tg} & u_{tg} & u_{tg} & * & * \\ p_{(t-1)gs_10} & z_{tgs_1} & z_{tgs_1} & o_{(t-1)gs_10} & * \\ y_{tgs_1} & p_{tgs_20} & y_{tgs_1} & h_{tgs_1s_2} & o_{tgs_20} \end{bmatrix} = \begin{bmatrix} x_{(t-1)g} \\ x_{tg} \\ u_{tg} \\ p_{(t-1)gs_10} \\ p_{tgs_10} \end{bmatrix} \begin{bmatrix} x_{(t-1)g} & x_{tg} & u_{tg} & p_{(t-1)gs_10} & p_{tgs_10} \end{bmatrix} \tag{2.24}$$

If equality holds at optimality, then the above relations are satisfied and the relaxation is regarded as exact. To further strengthen the proposed relaxation, we incorporate the Reformulation-Linearization Technique (RLT) technique [43]. Linear inequalities (2.22b) – (2.22e) are derived from (2.6). Lastly, inequalities (2.22g) – (2.22i) are immediate consequences of (2.5) and (2.6).

The variables that appear in (2.22) are tightly correlated and this is the primary motivation behind the proposed valid inequalities. In Section (2.5), we will demonstrate the effect of these additional inequalities on the quality of relaxation and their ability to obtain feasible points.

2.4 FEASIBLE POINT RECOVERY

Let $\{x^{\text{rlx}}_{tg}\}_{t\in\mathcal{T},\, g\in\mathcal{G}_t}$ denote the resulting schedule from a convex relaxation of SCUC. For large-scale problems, convex relaxations can fail to satisfy the integrality constraint (2.5). In this section, we propose a heuristic to infer a feasible point $\{\hat{x}_{tg} \in \{0,1\}\}_{t\in\mathcal{T},\, g\in\mathcal{G}_t}$. To this end, the main challenge is to ensure that the minimum up and minimum down constraints (2.7a) and (2.7b) are satisfied, which is not possible by simply rounding x^{rlx}_{tg} values. To tackle this issue we adopt the following procedure.

Feasible Point Recovery:

1) For every $t \in \mathcal{T}$ and $g \in \mathcal{G}_t$ do $x_{tg}^{\mathrm{rnd}} \leftarrow \mathrm{round}\{0.4 + x_{tg}^{\mathrm{rlx}}\}$.

2) For every $g \in \cup_{t\in\mathcal{T}} \mathcal{G}_t$,

(a) Solve the following linear program

$$\begin{aligned}
&\text{minimize} && \sum_{t\in\mathcal{T}} |x_{tg} - x_{tg}^{\mathrm{rnd}}| && && \text{(2.25a)}\\
&\text{subject to} && x_{tg} = 0 && \text{if} \quad g \notin \mathcal{G}_t && \text{(2.25b)}\\
& && 0 \le x_{tg} \le 1 && \text{if} \quad g \in \mathcal{G}_t && \text{(2.25c)}\\
& && x_{tg} \ge x_{\tau g} - x_{(\tau-1)g} && \forall t \in \mathcal{T},\ \forall \tau \in \{t - m_g^{\uparrow} + 1, \ldots, t\} && \text{(2.25d)}\\
& && 1 - x_{tg} \ge x_{(\tau-1)g} - x_{\tau g} && \forall t \in \mathcal{T},\ \forall \tau \in \{t - m_g^{\downarrow} + 1, \ldots, t\} && \text{(2.25e)}
\end{aligned}$$

and denote the resulting solution as $\{\hat{x}_{tg}\}_{t\in\mathcal{T}}$.

(b) For $t = 1, \ldots, |\mathcal{T}|$ do

$$\begin{aligned}
& a_{tg}^{\uparrow} \leftarrow \max\{\hat{x}_{\tau g} - \hat{x}_{(\tau-1)g} \mid \forall \tau \in \{t - m_g^{\uparrow} + 1, \ldots, t\}\}, && \text{(2.26a)}\\
& a_{tg}^{\downarrow} \leftarrow \max\{\hat{x}_{(\tau-1)g} - \hat{x}_{\tau g} \mid \forall \tau \in \{t - m_g^{\downarrow} + 1, \ldots, t\}\}, && \text{(2.26b)}\\
& \text{if} \quad a_{tg}^{\uparrow} = 0 \ \wedge\ a_{tg}^{\downarrow} = 0 \quad \text{then} \quad \hat{x}_{tg} \leftarrow x_{tg}^{\mathrm{rnd}}, && \text{(2.26c)}\\
& \text{if} \quad a_{tg}^{\uparrow} = 0 \ \wedge\ a_{tg}^{\downarrow} = 1 \quad \text{then} \quad \hat{x}_{tg} \leftarrow 0, && \text{(2.26d)}\\
& \text{if} \quad a_{tg}^{\uparrow} = 1 \ \wedge\ a_{tg}^{\downarrow} = 0 \quad \text{then} \quad \hat{x}_{tg} \leftarrow 1, && \text{(2.26e)}\\
& \text{if} \quad a_{tg}^{\uparrow} = 1 \ \wedge\ a_{tg}^{\downarrow} = 1 \quad \text{then declare failure.} && \text{(2.26f)}
\end{aligned}$$

3) Declare $\{\hat{x}_{tg}\}_{t\in\mathcal{T},\, g\in\mathcal{G}_t}$ as the recovered schedule and solve the convex optimization

$$\begin{aligned}
&\text{minimize} && \text{(2.1a)+(2.1b)+(2.1c)} && && (2.27a)\\
&\text{subject to} && x_{tg} = \hat{x}_{tg} && \forall t \in \mathcal{T},\ \ \forall g \in \mathcal{G}_t && (2.27b)\\
& && \text{(2.6)} - \text{(2.9)} && \forall t \in \mathcal{T},\ \ \forall g \in \mathcal{G}_t && (2.27c)\\
& && \text{(2.10)} && \forall t \in \mathcal{T} && (2.27d)
\end{aligned}$$

to obtain a feasible point:

$$\begin{aligned}
&\{\hat{x}_{tg},\ \hat{p}^{\text{contract}}_{tg},\ \hat{r}^{+}_{tg},\ \hat{r}^{-}_{tg},\ \hat{w}^{+}_{tg},\ \hat{w}^{-}_{tg} \in \mathbb{R}\}_{t\in\mathcal{T},\, g\in\mathcal{G}_t}\\
&\{\hat{p}_{tgsc}\}_{t\in\mathcal{T},\, g\in\mathcal{G}_t,\, s\in\mathcal{S}_t,\, c\in\mathcal{C}_{ts}}, \quad \left\{\hat{\boldsymbol{\theta}}_{tsc} \in \mathbb{R}^{|\mathcal{V}|}\right\}_{t\in\mathcal{T},\, s\in\mathcal{S}_t,\, c\in\mathcal{C}_{ts}}.
\end{aligned}$$

In case of infeasibility, declare failure.

As we will demonstrate in Section (2.5), this heuristic is able to obtain good quality feasible points for challenging instances of SCUC. We use the following measure to evaluate the quality of the resulting feasible points:

$$\text{Optimality Gap } \% = 100 \times \frac{\hat{\sigma} - \sigma^{\text{rlx}}}{\hat{\sigma}} \tag{2.28}$$

where σ^{rlx} and $\hat{\sigma}$ are the optimal objective values for convex relaxation and the recovery problem (2.27), respectively.

2.5 EXPERIMENTS

In this section, we demonstrate the performance of the proposed convex relaxation on a wide range of challenging SCUC problems. Simulations are performed on a 64-bit computer with an Intel 3.0 GHz, 12-core CPU and 256 GB RAM using MATLAB 2019a. The

solver MOSEK v8.0.0.60 [44] is used for convex optimization through CVX v2.1 [45, 46]. SCUC problems are formulated using the MATPOWER Optimal Scheduling Tool (MOST) v1.0.2 [47]. For comparison, CPLEX v12.9.0.0 [48] and GUROBI v9.0 are used for mixed-integer programming through MOST. We would like to emphasis that CPLEX and GUROBI may exhibit far better performance on the same problem, if applied differently. System operators and utility companies may leverage stronger MILP formulations and valid inequalities in order to strengthen the performance of SCUC.

2.5.1 Data

Transmission Network Data: We use IEEE and Pan European Grid Advanced Simulation and State Estimation (PEGASE) benchmark grids from MATPOWER [47]. Certain modifications are made to the following parts of the data in order to make the resulting SCUC problems feasible and sufficiently challenging:

- $\boldsymbol{f}_{tc}^{\max}$: Line thermal limits specified in MATPOWER data files were used without modifications. Source data on line flow limits are specified in the documentation of MATPOWER data files [47].
- $\boldsymbol{d}_{tc}$: With no loss of generality, we assume that all loads are deterministic and we do not consider the contingency of loads. In all of the simulations, load variations throughout the day, follow the vector:

$$\begin{aligned}\boldsymbol{\pi}^{\text{gen}} \triangleq \nu^{\text{gen}} \times [\, & 0.684,\ 0.645,\ 0.620,\ 0.604,\ 0.606,\ 0.627 \\ & 0.677,\ 0.694,\ 0.730,\ 0.808,\ 0.893,\ 0.922 \\ & 0.946,\ 0.952,\ 0.972,\ 0.999,\ 1.000,\ 0.964 \\ & 0.961,\ 0.927,\ 0.927,\ 0.909,\ 0.765,\ 0.764\,]\end{aligned}$$

where $\nu^{\text{gen}} = 0.9$ for case New England 39-bus system and $\nu^{\text{gen}} = 0.5$ for all of the other benchmark cases. In other words, for every $t \in \mathcal{T}$ and $c \in \cup_{s \in \mathcal{S}_t} \mathcal{C}_{ts}$ we have $\boldsymbol{d}_{tc} = \pi_t^{\text{gen}} \, \boldsymbol{d}$, where $\boldsymbol{d}$ is the vector of nodal demand from MATPOWER.

In addition to the above modifications, we have added wind generators to certain buses and altered generator costs due to the absence of fixed, quadratic, reserve and load-following costs in MATPOWER data. These changes are detailed next.

Deterministic Generator Cost Data:

- α_{tg}^{sqr}, α_{tg}^{lin}, ζ_{tg}, $\zeta_{tg}^{\uparrow}$, $\zeta_{tg}^{\downarrow}$: These cost coefficients are randomly chosen based on uniform distributions within $\pm 20\%$ of mean values \$0.0025/(MW.h)^2, \$20/(MW.h), \$500/h, \$5000/h, and \$500/h, respectively following [49, 50] .

- η_{tg}^{+}, η_{tg}^{-}, μ_{tg}^{+}, μ_{tg}^{-}: Reserve cost coefficients are selected as $\eta_{tg}^{+} = \eta_{tg}^{-} = 5.0 \, \alpha_{tg}^{\text{lin}}$ and $\mu_{tg}^{+} = \mu_{tg}^{-} = 0.2 \, \alpha_{tg}^{\text{lin}}$.

- β_{tg}^{+}, β_{tg}^{-}: Active power re-dispatch cost coefficients are selected as $\beta_{tg}^{+} = \beta_{tg}^{-} = 0.2 \, \alpha_{tg}^{\text{lin}}$.

- κ_g: Ramp "wear and tear" cost coefficients are selected as $\kappa_g = 500 \alpha_{tg}^{\text{sqr}}$.

Deterministic Generator Limits:

- $\underline{p}_g$: Minimum active power is selected as $\underline{p}_g = 0$.

- $m_g^{\uparrow}$, $m_g^{\downarrow}$: A quarter of the generators are randomly selected with $m_g^{\uparrow} = m_g^{\downarrow} = 1$ to act as fast-start units that have the capacity to ramp-up quickly in order to support generation shortfalls. For the remaining generators

$$m_g^{\uparrow} = \min \left\{ \tilde{m}_g^{\uparrow} + 1, \, \lfloor |\mathcal{T}|/2 \rfloor \right\}$$
$$m_g^{\downarrow} = \min \left\{ \tilde{m}_g^{\downarrow} + 1, \, \lfloor |\mathcal{T}|/2 \rfloor \right\}$$

where each $\tilde{m}_g^{\uparrow}$ and $\tilde{m}_g^{\downarrow}$ has Poisson distribution with parameter 4.

- The initial state of each generator is uniformly chosen from the set of integers $\{k \in \mathbb{Z} \mid -5 \leq k \leq 5\} \setminus \{0\}$ with negative and positive numbers, respectively, indicating the number of uptime and downtime periods at $t = 0$.

- $\bar{w}_{tg}$, $\underline{w}_{tg}$, $\bar{r}_{tg}$, $\underline{r}_{tg}$, $\bar{\Delta}_g$, $\underline{\Delta}_g$: Following [38], ramp limits are selected as $\bar{w}_{tg} = \underline{w}_{tg} = 0.3\bar{p}$ and $\bar{r}_{tg} = \underline{r}_{tg} = \bar{\Delta}_g = \underline{\Delta}_g = 0.1\bar{p}$.

Wind Generator Data: Data on wind generators and hourly wind profile are obtained from the SW Minnesota wind power plant [51]. Let $|\mathcal{G}|$ indicate the total number of deterministic generators. We consider $\mathrm{round}\{|\mathcal{G}|/3\}$ wind generators, each located at a randomly chosen bus. We consider 5 wind scenarios representing 100%, 80%, 60% 40%, and %20 wind generation, with initial probabilities

$$\Phi_1 = \begin{bmatrix} 0.11 & 0.48 & 0.17 & 0.17 & 0.07 \end{bmatrix}^{\top} \tag{2.29}$$

respectively. Additionally, for every $t \in \mathcal{T} \setminus \{1\}$ the transition probability matrix is set to

$$\Phi_t = \begin{bmatrix} 0.7858 & 0.2001 & 0.0109 & 0.0032 & 0 \\ 0.1022 & 0.6215 & 0.2381 & 0.0371 & 0.0012 \\ 0.0154 & 0.3184 & 0.5042 & 0.1439 & 0.0181 \\ 0.0022 & 0.0356 & 0.2488 & 0.5435 & 0.1698 \\ 0 & 0.0004 & 0.0073 & 0.0543 & 0.9379 \end{bmatrix} \tag{2.30}$$

The scenario transition probabilities $\phi_{ts_1s_2}$ are obtained from the SW Minnesota wind power plant [51]. The coefficients of (2.29) – (2.30) is used to weight ramp "wear and tear" cost in (2.1c).

- α_{tg}^{lin}, ζ_{tg}, $\zeta_{tg}^{\uparrow}$, $\zeta_{tg}^{\downarrow}$: Wind energy cost coefficients are selected as $\alpha_{tg}^{\text{lin}} =$ \$20/(MW.h), $\zeta_{tg} =$ \$20/h, and $\zeta_{tg}^{\uparrow} = \zeta_{tg}^{\downarrow} =$ \$0/h.

- Wind generator output is given by the product of the maximum wind generator output from MATPOWER [52] and the ratios

$$\begin{aligned}\boldsymbol{\pi}^{\text{wind}} \triangleq [&0.72,\ 0.61,\ 0.35,\ 0.28,\ 0.15,\ 0.39\\ &0.25,\ 0.35,\ 0.29,\ 0.57,\ 0.49,\ 0.37\\ &0.52,\ 0.34,\ 0.42,\ 0.41,\ 0.63,\ 0.42\\ &0.29,\ 0.53,\ 0.79,\ 0.83,\ 0.81,\ 0.87]\end{aligned}$$

Contingencies: We consider N-1 contingency analysis in this study. 3 generators and 3 lines are randomly selected each representing a contingency with probability $1/60$.

- ψ_{tsc}: Base scenario conditional probabilities are selected as $\psi_{ts0} = 0.1/|\mathcal{C}|$ for every $s \in \mathcal{S}$. Additionally, for every $c \in \mathcal{C}$ post-contingency probabilities are given by:

$$\begin{bmatrix}\psi_{t1c}\\ \psi_{t2c}\\ \vdots\\ \psi_{t|\mathcal{S}|c}\end{bmatrix} = \frac{1}{|\mathcal{C}|} \times \Phi_t \begin{bmatrix}\psi_{(t-1)10}\\ \psi_{(t-1)20}\\ \vdots\\ \psi_{(t-1)|\mathcal{S}|0}\end{bmatrix} \tag{2.31}$$

- γ_t: Lastly, the probability of making it to period t without branching off the central path in a contingency is given by:

$$\gamma_t = \sum_{s\in\mathcal{S}_t} \psi_{(t-1)s0} \qquad = \sum_{s\in\mathcal{S}_t,\, c\in\mathcal{C}_{ts}} \psi_{tsc} \leq 1, \text{ for } t \geq 1 \tag{2.32}$$

2.5.2 Evaluation of Lower Bound

In order to evaluate the performance of our proposed SDP relaxation, we consider 5 benchmark grids based on IEEE and PEGASE modified data. Each benchmark grid is simulated in 4 realizations producing 20 test cases. The planning horizon is divided into 24 hourly intervals, 6 stochastic wind scenarios and 6 independent contingencies. The largest grid considered is PEGASE 2869 benchmark grid with 2,869 buses (vertices) and 510 generating units. For the largest benchmark, the model has 12,240 binary decision variables and 1,830,560 continuous variables. Table 2.1 presents details on the benchmark grids.

Table 2.2 reports performance of SDP relaxation compared to CPLEX and GUROBI numerical solvers and also perspective and LP relaxation methods. Performance is compared in terms of: i) convex lower bound (LB) on the optimal cost, ii) cost of the recovered feasible solution, iii) optimality gap and iv) computation time $t(s)$. In all experiments performed using SDP relaxation, we successfully infer a feasible point using heuristics presented in Section (2.4). The reported gaps in Table 2.2 show that SDP relaxation achieves average of 0.05% and does not exceed 0.36% optimality gap for all the test cases. This is better than average gap reported by both perspective and LP relaxations. Computation time reported by SDP relaxation averages at 35 mins. 35 sec.

2.5.3 Solution Quality

Figures 2.1a and 2.2a emphasize disparities in the number of inexact binaries generated by SDP, perspective and LP methods of relaxation for large test cases such as PEGASE 1354 and PEGASE 2869. As shown in Figures 2.1a and 2.2a, SDP relaxation generates fewer inexact binaries between '0' and '1' as compared to perspective and LP relaxations. Figures 2.1b, 2.1c, 2.2b and 2.2c shows that perspective and LP relaxations report higher number of inexact binaries. Poor solution quality negatively impacts ability of the proposed heuristic to infer a feasible point resulting in failed recoveries. Table 2.2 shows failed re-

Table 2.1: Experiments for 24-hour horizon scheduling of benchmark systems

Experiment	Test Cases	# of Generators	# of Binaries	# of Continuous variables
1	New England 39-bus	10	240	67,750
2	New England 39-bus	10	240	67,750
3	New England 39-bus	10	240	67,750
4	New England 39-bus	10	240	67,750
5	IEEE 118	54	1,296	191,664
6	IEEE 118	54	1,296	191,664
7	IEEE 118	54	1,296	191,664
8	IEEE 118	54	1,296	191,664
9	IEEE 300	69	1,656	247,664
10	IEEE 300	69	1,656	247,664
11	IEEE 300	69	1,656	247,664
12	IEEE 300	69	1,656	247,664
13	PEGASE 1354	260	6,240	928,925
14	PEGASE 1354	260	6,240	928,925
15	PEGASE 1354	260	6,240	928,925
16	PEGASE 1354	260	6,240	928,925
17	PEGASE 2869	510	12,240	1,830,560
18	PEGASE 2869	510	12,240	1,830,560
19	PEGASE 2869	510	12,240	1,830,560
20	PEGASE 2869	510	12,240	1,830,560

coveries in experiments 15, 17 and 19 using perspective relaxation and experiments 14, 15 and 19 using LP relaxation due to poor solution quality. As seen from the table, all experiments using SDP relaxation produced feasible solutions because of fewer inexact binaries.

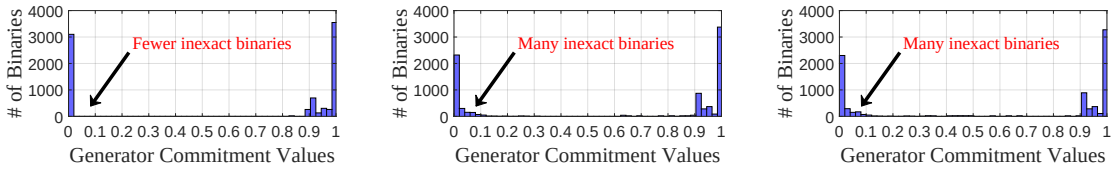

(a) SDP relaxation (b) Perspective relaxation (c) LP relaxation

Figure 2.1: Distribution of Binary variables for PEGASE 1354 (Experiment 14) in 24-hour horizon scheduling

Table 2.2: The performance of SDP relaxation algorithm for 24-hour horizon scheduling of benchmark systems (4 realizations in each benchmark system)

Exp.	Test Case	CPLEX			GUROBI			SDP Relaxation					Perspective Relaxation					LP Relaxation				
		Feasible	GAP (%)	t(s)	Feasible	GAP (%)	t(s)	LB	Feasible	GAP (%)	Determined Binaries (%)	t(s)	LB	Feasible	GAP (%)	Determined Binaries (%)	t(s)	LB	Feasible	GAP (%)	Determined Binaries (%)	t(s)
1	NE 39 bus	-2.621e+6	0.00	94.26	-2.621e+6	0.00	442.81	-2.621e+6	-2.621e+6	0.002	100	42.7	-2.623e+6	-2.620e+6	0.076	92.92	7.55	-2.627e+6	-2.620e+6	0.153	92.92	7.05
2	NE 39 bus	-1.337e+6	0.00	119.59	-1.337e+6	0.00	473.75	-1.337e+6	-1.337e+6	0.008	99.58	39.78	-1.339e+6	-1.337e+6	0.147	96.67	7.05	-1.340e+6	-1.337e+6	0.055	96.67	6.06
3	NE 39 bus	-1.867e+6	0.15	81.94	-1.867e+6	0.00	247.77	-1.867e+6	-1.867e+6	0.020	98.75	30.7	-1.871e+6	-1.867e+6	0.174	85	7.53	-1.873e+6	-1.867e+6	0.123	85	6.88
4	NE 39 bus	-2.149e+6	0.08	163.27	-2.149e+6	0.00	588.68	-2.150e+6	-2.149e+6	0.065	97.92	33.67	-2.152e+6	-2.149e+6	0.064	90.42	8.16	-2.159e+6	-2.149e+6	0.331	90.42	6.11
5	IEEE 118	–	–	3,600†	–	–	3,600†	-5.592e+5	-5.592e+5	6.496e-4	100	721.7	-5.592e+5	-5.592e+5	3.493e-5	100	40.8	-5.621e+5	-5.592e+5	0.518	100	38.34
6	IEEE 118	–	–	3,600†	–	–	3,600†	-8.022e+5	-8.022e+5	4.642e-4	100	879.89	-8.022e+5	-8.022e+5	4.053e-6	100	46.56	-8.062e+5	-8.022e+5	0.491	100	40.19
7	IEEE 118	–	–	3,600†	–	–	3,600†	-9.297e+5	-9.297e+5	5.577e-5	100	789.39	-9.297e+5	-9.297e+5	3.270e-6	100	38.17	-9.304e+5	-9.297e+5	0.073	100	39.94
8	IEEE 118	–	–	3,600†	–	–	3,600†	-3.064e+5	-3.064e+5	2.006e-4	100	783.75	-3.064e+5	-3.064e+5	6.499e-4	100	46.38	-3.145e+5	-3.064e+5	2.646	100	41.69
9	IEEE 300	–	–	3,600†	–	–	3,600†	-9.214e+6	-9.208e+6	0.069	93.78	1,128.7	-9.215e+6	-9.207e+6	0.016	93.12	67.89	-9.229e+6	-9.207e+6	0.145	93.12	51.25
10	IEEE 300	–	–	3,600†	–	–	3,600†	-3.498e+6	-3.498e+6	2.903e-4	100	1,071.2	-3.501e+6	-3.497e+6	0.070	98.25	52.23	-3.516e+6	-3.497e+6	0.446	98.25	47.7
11	IEEE 300	–	–	3,600†	–	–	3,600†	-6.558e+6	-6.558e+6	1.012e-4	100	1,279.2	-6.560e+6	-6.555e+6	0.028	96.01	47.59	-6.574e+6	-6.555e+6	0.220	96.01	39.88
12	IEEE 300	–	–	3,600†	–	–	3,600†	-8.045e+6	-8.040e+6	0.057	95.59	1,291.5	-8.048e+6	-8.038e+6	0.032	93.06	56.06	-8.060e+6	-8.038e+6	0.158	93.06	50.77
13	PEGASE 1354	–	–	3,600†	–	–	3,600†	-3.463e+7	-3.459e+7	0.129	97.76	6,444.9	-3.470e+7	-9.231e+6	0.194	91.55	364.22	-3.488e+7	-9.886e+6	0.512	91.55	298.52
14	PEGASE 1354	–	–	3,600†	–	–	3,600†	-3.441e+7	-3.440e+7	0.003	99.63	9,278.9	-3.447e+7	-9.828e+6	0.184	94.38	400.83	-3.457e+7	–	0.303	94.38	301.88
15	PEGASE 1354	–	–	3,600†	–	–	3,600†	-2.827e+7	-2.826e+7	0.036	97.45	5,496.4	-2.834e+7	–	0.238	91.43	347.55	-2.851e+7	–	0.604	91.43	279.64
16	PEGASE 1354	–	–	3,600†	–	–	3,600†	-3.837e+7	-3.823e+7	0.354	96.39	6,203.6	-3.849e+7	-1.282e+7	0.323	90.79	368.33	-3.864e+7	-1.363e+7	0.374	90.79	321.2
17	PEGASE 2869	–	–	3,600†	–	–	3,600†	-4.753e+7	-4.751e+7	0.025	98.59	1,311.8	-4.760e+7	–	0.149	92.51	568.5	-4.787e+7	2.414e+6	0.565	92.51	425.47
18	PEGASE 2869	–	–	3,600†	–	–	3,600†	-5.420e+7	-5.415e+7	0.090	98.38	1,529.8	-5.429e+7	-1.310e+6	0.174	92.38	600.66	-5.450e+7	-1.861e+6	0.378	92.38	425.17
19	PEGASE 2869	–	–	3,600†	–	–	3,600†	-5.394e+7	-5.393e+7	0.031	98.44	1,600.5	-5.310e+7	–	0.102	94.14	534.64	-5.412e+7	–	0.235	94.14	433.41
20	PEGASE 2869	–	–	3,600†	–	–	3,600†	-5.402e+7	-5.400e+7	0.027	98.22	2,755.3	-5.410e+7	-3.900e+6	0.147	92.94	399.14	-5.420e+7	-4.629e+6	0.1861	92.94	436.77
Avg			–	–		–	–			0.046		2,135.7			0.106		200.49			0.426		164.90
Max			–	–		–	–			0.354		2,755.3			0.323		600.66			2.646		436.77

† Solvers are terminated within 3600 seconds.

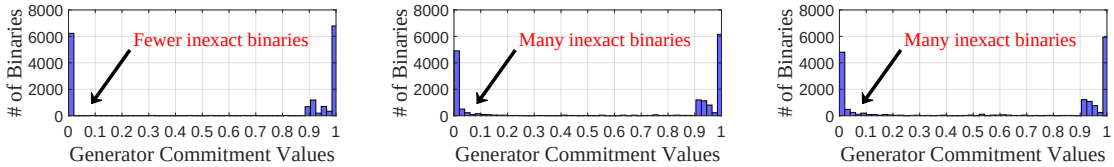

(a) SDP relaxation (b) Perspective relaxation (c) LP relaxation

Figure 2.2: Distribution of Binary variables for PEGASE 2869 (Experiment 17) in 24-hour horizon scheduling

2.5.4 Hourly Profile

Fig. 2.3 depicts the 24-hr profile of selected generators and transmission lines in SCUC experiment 1 on New-England 39 bus benchmark system. The data and the resulting commitment keys for this particular experiment are given by Tables 2.3 and 2.4. In the figure, Gen. #5 and line #38 are shown in pre and post-contingency states, and Gen. #2 in post-contingency state. Post-contingency #1 represents outage of Gen. #3 while post-contingency #6 represents loss of line #35. In Fig. 2.3, hourly profile is divided into 3 scenarios with probability assigned to transition from one scenario to the other. Notice that during on-peak hours 12PM – 10PM, Gen. #2 drives up to maximum output power in order to supply peak load in pre and post-contingency states. Likewise, Gen. #5 sees a significant

Table 2.3: Generator data for New England 39-bus benchmark system (Experiment 1)

Unit	Gen. #1	Gen. #2	Gen. #3	Gen. #4	Gen. #5	Gen. #6	Gen. #7	Gen. #8	Gen. #9	Gen. #10	Wnd. #1	Wnd. #2	Wnd. #3
α_{tg}^{sqr} ($/MW^{2}h)	0.0026	0.0022	0.0013	0.0018	0.0009	0.002	0.0018	0.0019	0.0038	0.0026	0	0	0
α_{tg}^{lin} ($/MWh)	20.68	28.78	7.85	24.01	15.09	14.71	22.39	31.65	10.35	25.52	20	20	20
ζ_{tg} ($/h)	821.47	259.33	338.63	497.22	811.92	501.13	321.60	527.17	559.40	430.24	20	20	20
$\zeta_{tg}^{\uparrow}$ ($/h)	1,118.1	6,622.1	5,054	4,050.1	1,519.5	3,868.6	2,874	2,628	7,510.2	4,147.5	0	0	0
$\zeta_{tg}^{\downarrow}$ ($/h)	142.86	400.04	720	232.24	829.78	355.36	363.82	263.39	713.77	155.98	0	0	0
μ_{tg}^{+}, μ_{tg}^{-} ($/MWh)	4.13	5.75	1.56	4.80	3.01	2.94	4.47	6.32	2.07	5.10	4	4	4
η_{tg}^{+}, η_{tg}^{-} ($/MWh)	4.30	5.82	3.66	6.64	1.35	7.19	5.46	4.37	1.71	6.16	4	4	4
β_{tg}^{+}, β_{tg}^{-} ($/MWh)	103.37	143.88	39.24	120.07	75.46	73.53	111.93	158.23	51.77	127.59	100	100	100
κ_g ($/MW^{2}h)	1.29	1.10	0.66	0.89	0.47	1	0.91	0.93	1.88	1.31	0	0	0
Pmax (MW)	1040	646	725	652	508	687	580	564	865	1100	100	100	100
Pmin (MW)	0	0	0	0	0	0	0	0	0	0	0	0	0
$m_g^{\uparrow}$ (h)	7	5	10	7	1	7	10	7	1	1	1	1	1
$m_g^{\downarrow}$ (h)	3	10	4	7	1	4	5	10	1	1	1	1	1
Initial state (h)	5	-3	-4	3	3	-1	1	4	4	-1	1	1	1

Table 2.4: Binary commitment decisions for New England 39-bus benchmark system (Experiment 1)

Cost: $604,856.05																								
Unit	1	2	3	4	5	6	7	8	9	10	11	12	13	14	15	16	17	18	19	20	21	22	23	24
Gen. #1	1	1	1	1	1	1	1	1	1	1	1	1	1	1	1	1	1	1	1	1	1	1	1	1
Gen. #2	0	0	0	0	0	0	0	1	1	1	1	1	1	1	1	1	1	1	1	1	1	1	1	1
Gen. #3	1	1	1	1	1	1	1	1	1	1	1	1	1	1	1	1	1	1	1	1	1	1	1	1
Gen. #4	1	1	1	1	1	1	1	1	1	1	1	1	1	1	1	1	1	1	1	1	1	1	1	1
Gen. #5	1	1	1	1	1	1	1	1	1	1	1	1	1	1	1	1	1	1	1	1	1	1	1	1
Gen. #6	0	0	0	1	1	1	1	1	1	1	1	1	1	1	1	1	1	1	1	1	1	1	1	1
Gen. #7	1	1	1	1	1	1	1	1	1	1	1	1	1	1	1	1	1	1	1	1	1	1	1	1
Gen. #8	1	1	1	1	1	1	1	1	1	1	1	1	1	1	1	1	1	1	1	1	1	1	1	1
Gen. #9	1	1	1	1	1	1	1	1	1	1	1	1	1	1	1	1	1	1	1	1	1	1	1	1
Gen. #10	1	1	1	1	1	1	1	1	1	1	1	1	1	1	1	1	1	1	1	1	1	1	1	1
Wnd. #1	1	1	1	1	1	1	1	1	1	1	1	1	1	1	1	1	1	1	1	1	1	1	1	1
Wnd. #2	1	1	1	1	1	1	1	1	1	1	1	1	1	1	1	1	1	1	1	1	1	1	1	1
Wnd. #3	1	1	1	1	1	1	1	1	1	1	1	1	1	1	1	1	1	1	1	1	1	1	1	1

upward climb in output power in post-contingency #1 in order to compensate for outage to Gen. #3. This presents stress on the network which is discussed next and illustrated by 2.4.

As seen in Fig. 2.3, line #38 shows signs of congestion in post-contingency #6 due to loss of line #35 during on-peak hours. Of significance, line flows in post-contingency state is almost three times higher than line flows before contingency occurred. The impact of high wind penetration on generator and line congestion is seen between 9PM – 1AM. Between 9PM – 1AM, wind penetration is at its highest point coinciding with congested generators and line flows. This results in the noticeable decline in line flows and power generation seen between 9PM – 1AM in Fig. 2.3.

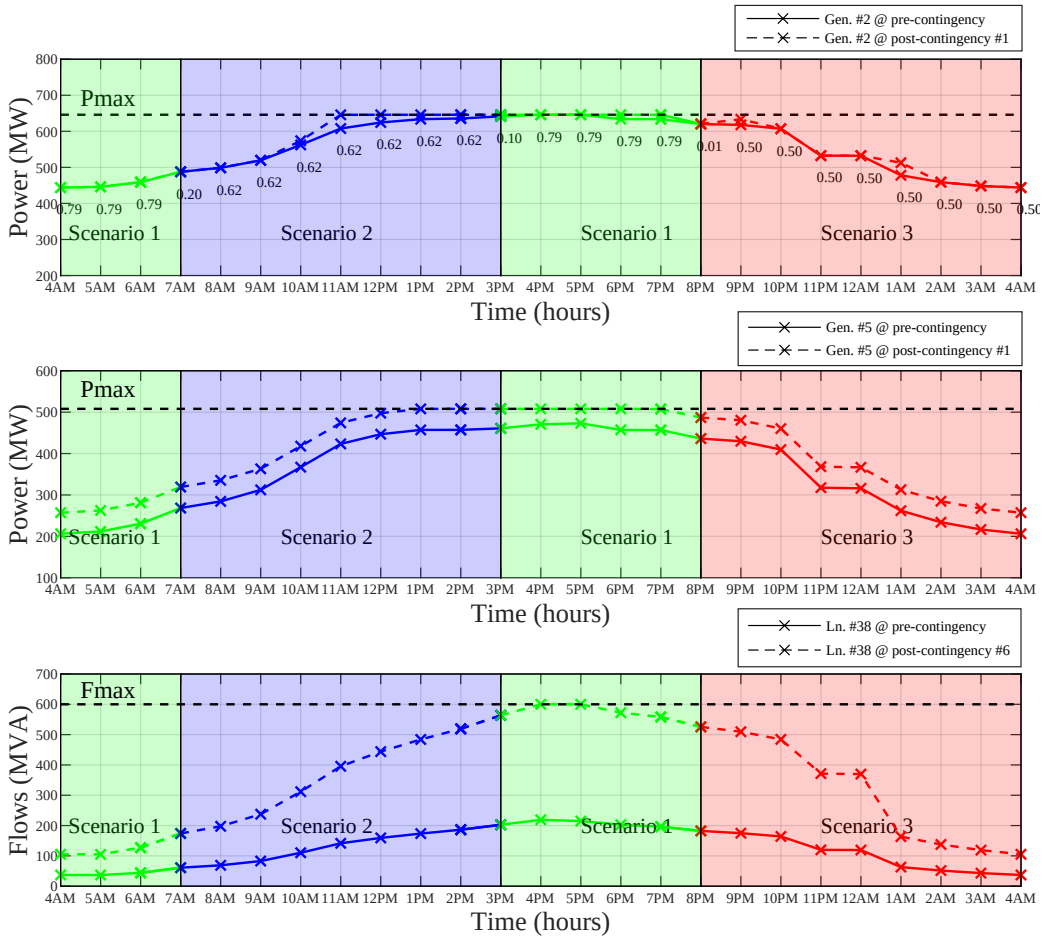

Figure 2.3: New-England 39-bus (Experiment 1) 24-hr profile showing generator output and line flows. First from top: Gen. 2 base case and post-contingency power output showing transition probabilities across 3 scenarios. Second from top: Gen. 5 base case and post-contingency power output across 3 scenarios. Third from top: Line 38 basecase and post-contingency power flows across 3 scenarios.

2.5.5 Network Congestion

Fig. 2.4 shows the contrast in network congestion between pre and post-contingency states of New England 39-bus benchmark grid. As seen in Fig. 2.4a, all 46 transmission lines operate within thermal limits with some lines transmitting more power than others as indicated by varying thickness of lines in the figure. Directional arrows are used to show the flow of power throughout the grid network.

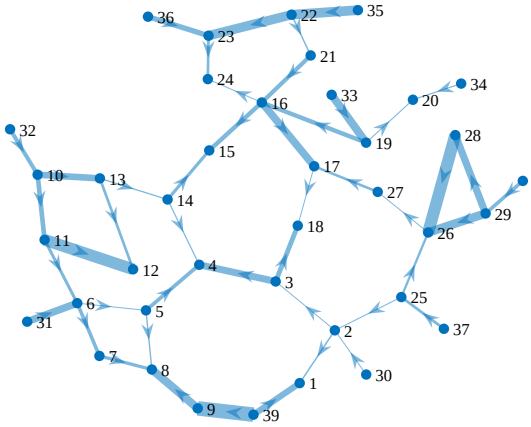

(a) Pre-contingency case @ 4PM , high wind penetr tion, no contingency

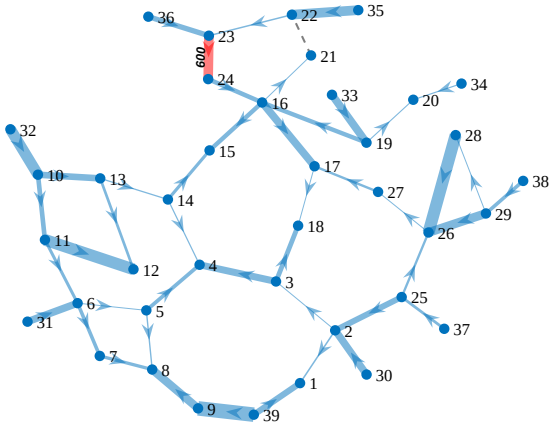

(b) Post-contingency case @ 4PM, high wind penetration, line contingency @ line 22 $\rightarrow$ 21. As a result of the contingnecy, line 23 $\rightarrow$ 24 is congested.

Figure 2.4: Directed graph of New England 39-bus Pre and Post-contingencies

In post-contingency state #6 depicted in Fig. 2.4b, we observe network congestion during peak hours of the day. The loss of line #35 in this contingency results in congestion on transmission line connecting bus 23 to 24 at severe levels attributed to increased flow of power in order to supply peak load at bus 24. The contingency also results in reversal of flow on line connecting bus 16 to 21 and line connecting bus 16 to 24. Power flow is increased on neighboring lines in attempts to compensate for loss of line #35 as observed in line from bus 22 to bus 23, as well as bus 32 to bus 10 to mention a few.

We observe that line contingencies make the SCUC problem more challenging since power flow is redirected to compensate for the sudden loss of a line or a generator. Since line flows must not exceed the maximum thermal limits, lines tend to become congested and in some cases reach critical levels.

2.6 CONCLUSIONS

In this paper, we study the SCUC problem under uncertainty by adopting a stochastic formulation proposed in [34]. The proposed method for tackling the computationally chal-

lenging problem is tested extensively on IEEE and PEGASE benchmark systems to establish its relative performance against two widely used off-the-shelf solvers, CPLEX and GUROBI and common-practice methods of relaxation, namely perspective and LP relaxations. It is shown that SDP relaxation consistently finds near-globally optimal solutions in each benchmark system under uncertain wind scenarios and with an extensive list of contingencies with up to 12,240 binary variables and 1,830,560 continuous variables.

CHAPTER 3

PROACTIVE POSTURING OF LARGE POWER GRID FOR MITIGATING HURRICANE IMPACTS

Proactive Posturing of Large Power Grid for Mitigating Hurricane Impacts[1]

E. Quarm Jnr., X. Fan, M.A. Elizondo, and R. Madani. "Proactive Posturing of Large Power Grid for Mitigating Hurricane Impacts." – To appear in 2022 IEEE PES Conference on Innovative Smart Grid Technologies (ISGT 2022).

Proactive Posturing of Large Power Grid for Mitigating Hurricane Impacts

Edward Quarm Jnr.[1,2], Xiaoyuan Fan[2], Marcelo Elizondo[2] and Ramtin Madani[1]

[1]Department of Electrical Engineering, University of Texas at Arlington, TX, USA.

[2]Energy and Environment Directorate, Pacific Northwest National Laboratory, WA, USA

Abstract — In the past decade, natural disasters such as hurricanes have challenged the operation and control of U.S. power grid. It is crucial to develop proactive strategies to assist grid operators for better emergency response and minimized electricity service interruptions. In this paper, we propose a proactive posturing of power system elements, and formulated a Security-Constrained Optimal Power Flow (SCOPF) informed by cross-domain hurricane modeling and its potential impacts on grid elements. Simulation results based on real-world power grid and historical hurricane event validated the applicability of the proposed optimization formulation, and show potential to enable grid operators and planners with interactive cross-domain data analytics for mitigating hurricane impacts.

Keywords — Power system emergency response, security constrained optimal power flow, hurricane impact mitigation.

3.1 INTRODUCTION

Severe weather is one of the major threats to power system security in the United States today. The effects of climate change and worsening pollution levels have contributed to destructive weather events such as hurricanes, tornadoes, blizzards, and droughts [53]. Therefore, it is crucial to develop a framework for establishing critical infrastructure resilience goals [54], and using it as one important guideline for multi-domain, multi-agency coordination, planning, and emergency response. For example, in 2017, Hurricane Irma and Maria stroke Puerto Rico as Category 5 storm, and caused prolonged yet wide-spread damage to Puerto Rico's electrical infrastructure. Since then, research efforts have been made to develop new algorithms and tools in support of optimized grid resilience improvements and potential emergency mitigation strategies [55, 56].

Several research papers have explored different ways of including hurricane contingencies into the optimal power flow (OPF) and unit commitment (UC) problems. Current modeling approaches can be widely classified into two categories: proactive operation, and corrective operation of the grid in response to contingency events. Studies [57–59] explored corrective approaches to contingency modeling where [60–62] explored proactive approaches. Proactive modeling strategies such as [62] has shown some promise in mitigating the adverse impacts of contingencies on the grid.

Large-scale SCOPF problems are computationally intractable [63,64]. The complexity is attributed to the presence of nonlinear alternating current (AC) network constraints, enforcing large number of transmission constraints, considering multiple scenarios and multiple contingencies in the formulation [65, 66]. In order to alleviate the computational burden in $N - k$ OPF problems, research papers [65, 67] proposed contingency screening to reduce problem size.

Semi-definite programming (SDP) relaxation holds significant promise for application to large-scale OPF and UC problems. In [68], the authors proved that a global opti-

mum solution to the OPF problem can be obtained when the duality gap is zero. However, for some practical problems SDP relaxation may not be tight, therefore, fails to obtain a global optimum solution. In order to address inexactness of SDP relaxation, penalty terms are incorporated into the objective of convex relaxations to drive the solution to near-globally optimal solution [66,69–71]. Furthermore, [72] proposed adding valid inequalities to strengthen SDP relaxation when the relaxation is inexact.

Very few papers have attempted to consider the sequential temporal relationship between individual contingencies in the multi-period SCOPF problem. In this paper, we adopt a proactive strategy of handling contingencies brought about by hurricane events with the aim of improving the preparedness of the grid to withstand the disruptive events. The temporal relations among individual steps (groups of time period) within one hurricane event have been explored, in particular the present group of power system contingencies (includes outaged generators and transmission line) will be considered as N-1 security constraints, while the following group of power system contingencies is incorporated as explicit line rating constraints; this cascaded forward-looking design embodies proactive posturing of power system elements, but differentiates itself from simply stacking adjacent groups of power system contingencies. To tackle this, We employ a low order conic relaxation which has been demonstrated through multiple experiments in [73] to be exact for many large-scale SCUC problem and suitable to be applied to SCOPF formulations.

The rest of this paper is organized as follows: section 3.2 introduces modeling hurricane's impact on the electric grid. Next, the SCOPF with contingencies is formulated in 3.2.2. Numerical simulations are provided in section 3.3 and conclusions are summarized in section 3.4.

3.1.1 Notations

Throughout this paper, matrices, vectors and scalars are represented by boldface uppercase, boldface lowercase and italic lowercase letters, respectively. $|\cdot|$ represents the absolute value of a scalar or the cardinality of a set. The symbol $(\cdot)^\top$ represents the transpose operator. The notation real$\{\cdot\}$ represents the real part of a scalar or a matrix. Given a matrix $\boldsymbol{A}$, the notation $\boldsymbol{A}$, the notation $\boldsymbol{A}_{jk}$ refers to its $(j,k)^{th}$ element. $\boldsymbol{A}$, he notation $\boldsymbol{A}_{jk}$ refers to its $(j,k)^{th}$ element. $\boldsymbol{A} \succeq 0$ means that $\boldsymbol{A}$ is symmetric and positive semidefinite.

3.2 MODELING HURRICANE'S IMPACT ON GRID AND THE OPTIMIZATION PROBLEM FORMULATION

As one of the major natural disasters that influence U.S. every year, the modeling and prediction of hurricane based on climatology and meteorology are critical and fundamental [74]. But to fully capture its impacts on power grid and further take advantage of such cross-domain capabilities into power grid operation and planning, major barriers including GIS data fusion and standardized cross-domain data curation pose significant challenges for private industry [56], not even mention the following requirements on optimization and computing techniques when developing system hardening strategies and impact mitigation plan.

To overcome those challenges, we formulate a multi-period SCOPF problem, which considers hurricane-influenced grid contingencies as well as the sequential temporal relationship between individual steps. As a result, the modeling and prediction of hurricane, usually published 24 to 72 hours in advance, can be transformed into cross-domain intelligence in a proactive manner, and further incorporated into power system domain analysis. More details are given as follows.

3.2.1 Hurricane Contingency Description

Hurricane can be modelled as a multi-step temporal process, each step includes the damaged group of power system equipment and may be described as classical contingency for power grid, such as line tripping, generation tripping, etc.. It should be noted that individual power system equipment has its own fragility curve, which dictates the failure possibility of that equipment under certain wind speed during hurricane or storm [55]. For example, one performed simulation for Hurricane Maria included three steps, and each step includes one PSS®E idv file to represent the sequence of elements damaged by hurricane. Therefore, each idv file is considered as a form of dynamic contingency simulation with proper time spacing between individual equipment failure, while it is also natural to be considered as $N - k$ contingency formulation in steady-sate analysis.

A preventive SCOPF problem can be formulated for each step, by taking advantage of temporal relationship among the cascaded hurricane contingency groups and maximize the benefits of the predictable hurricane trajectory and intensity in advance. More specifically, by proactively posturing the power system operating conditions to embrace the possible grid contingencies due to power system equipment failure from both temporal and geographical perspectives, the proposed method aims to explore the optimal system operation point considering the current group of contingencies as security constraints, while also minimizing the potential impacts of the following batch of contingencies by penalizing line flows on candidate lines accordingly. As a result, the cross-domain intelligence from advanced hurricane modeling and prediction can be transformed into timely absorbable information to guide proactive posturing of power grid.

3.2.2 Multi-period Proactive SCOPF Problem Formulation

Let $\mathcal{T}$ represent the set of discrete time slots, with index t. Additionally, let $\mathcal{G}_t$ represent the set of all generating units that are available at time $t \in \mathcal{T}$. Define $\mathcal{C}_t$ as the

set of all predicted hurricane contingency cases with $0 \in \mathcal{C}_t$ representing the base case (normal grid operation). Lastly, $\mathcal{G}_{tc} \subseteq \mathcal{G}_t$ is defined as the set of all generating units that are available at time $t \in \mathcal{T}$ and contingency $c \in \mathcal{C}_t$, such that

$$\mathcal{G}_t = \cup_{c \in \mathcal{C}_t} \mathcal{G}_{tc}.$$

Consider a power system with $\mathcal{V}$ as the set of buses, and $\mathcal{E}_{tc} \subseteq \mathcal{V} \times \mathcal{V}$ as the set of branches at time $t \in \mathcal{T}$ and contingency $c \in \mathcal{C}_t$. The proactive SCOPF problem is formulated as:

$$\begin{aligned}
\text{min} \quad & \sum_{t \in \mathcal{T}} \Bigg(\sum_{c \in \mathcal{C}_t} \sum_{g \in \mathcal{G}_{tc}} \alpha_{tg}^{\text{sqr}} \, p_{tgc}^2 + \alpha_{tg}^{\text{lin}} \, p_{tgc} + \zeta_{tg} && \text{(3.1a)} \\
& + \sum_{c \in 0} \sum_{g \in \mathcal{G}_{tc}} \kappa_g \times \left(p_{tg0} - p_{(t-1)g0} \right)^2 && \text{(3.1b)} \\
& + \sum_{g \in \mathcal{G}_t} \Big(\eta_{tg}^{+} \, r_{tg}^{+} + \eta_{tg}^{-} \, r_{tg}^{-} && \text{(3.1c)} \\
& \qquad + \mu_{tg}^{+} \, w_{tg}^{+} + \mu_{tg}^{-} \, w_{tg}^{-} \Big) \Bigg) && \text{(3.1d)} \\
\text{s.t.} \quad & \boldsymbol{d}_{tc} + \boldsymbol{B}_{tc} \, \boldsymbol{\theta}_{tc} = \boldsymbol{C}_{tc}^{\top} \, \boldsymbol{p}_{tc}, \qquad \forall t, \forall c && \text{(3.1e)}
\end{aligned}$$

where

$$\boldsymbol{p}_{tc} \triangleq [p_{t1c}, \; p_{t2c}, \; \ldots, \; p_{t|\mathcal{G}_{tc}|c}]^{\top}$$

$$|\vec{\boldsymbol{B}}_{tc} \, \boldsymbol{\theta}_{tc} + \boldsymbol{f}_{tc}^{\text{shift}}| \leq \boldsymbol{f}_{tc}^{\max}, \qquad \forall t, \forall c \qquad \text{(3.1f)}$$

$$p_{gc}^{\min} \leq p_{tgc} \leq p_{gc}^{\max}, \qquad \forall t, \forall g, \forall c \qquad \text{(3.1g)}$$

$$0 \leq w_{tg}^{+} \leq w_{tg}^{\max}, \qquad \forall t, \forall g \qquad \text{(3.1h)}$$

$$0 \leq w_{tg}^{-} \leq w_{tg}^{\min}, \qquad \forall t, \forall g \qquad \text{(3.1i)}$$

$$p_{tg0} - p_{(t-1)g0} \leq w^{+}_{(t-1)g}, \qquad \forall t, \forall g \tag{3.1j}$$

$$p_{(t-1)g0} - p_{tg0} \leq w^{-}_{(t-1)g}, \qquad \forall t, \forall g \tag{3.1k}$$

$$0 \leq r^{+}_{tg} \leq r^{\max}_{tg}, \qquad \forall t, \forall g \tag{3.1l}$$

$$0 \leq r^{-}_{tg} \leq r^{\min}_{tg}, \qquad \forall t, \forall g \tag{3.1m}$$

$$p_{tgc} - p_{tg0} \leq r^{+}_{tg}, \qquad \forall t, \forall g, \forall c \neq 0 \tag{3.1n}$$

$$p_{tg0} - p_{tgc} \leq r^{+}_{tg}, \qquad \forall t, \forall g, \forall c \neq 0 \tag{3.1o}$$

$$-\Delta^{\min}_{g} \leq p_{tgc} - p_{tg0} \leq \Delta^{\max}_{g}, \qquad \forall t, \forall g, \forall c \neq 0 \tag{3.1p}$$

Objective (3.1a) represents the operation cost with quadratic coefficient α^{sqr}_{tg}, linear coefficient α^{lin}_{tg} and fixed cost ζ_{tg}. (3.1b) represents the quadratic load-following ramp "wear and tear" cost with coefficient κ_g. Furthermore, (3.1c) accounts for the cost of contingency with coefficients η^{+}_{tg} and η^{-}_{tg}. Expression (3.1d) represents cost of load-following ramping reserves with coefficients μ^{+}_{tg} and μ^{-}_{tg}. Constraint (3.1e) imposes the Direct Current (DC) power balance constraints. Constraint (3.1f) restricts the flow of power by the vector of line thermal limits $\boldsymbol{f}^{\max}_{tc} \in \mathbb{R}^{|\mathcal{E}_{tc}|}$, where $\boldsymbol{f}^{\text{shift}}_{tc}$ accounts for the effect of transformers and phase shifters. Constraint (3.1g) imposes upper and lower limits $\{p^{\min}_{gc}, p^{\max}_{gc}\}$ on each generator. Per-period ramp limits are imposed on the units with constraints (3.1h) – (3.1k). Constraints (3.1l) – (3.1o) impose upward/downward limits $\{r^{\max}_{tg}, r^{\min}_{tg}\}$ on post-contingency dispatch quantities, respectively. Additionally, constraint (3.1p) enforces limits on downward and upward transitions from base to post-contingency state.

3.2.3 Multi-Step Cascaded Optimization Problem considering Hurricane Progression

A hurricane can be divided into multiple steps considering its time progression. In this case, the resulted power flow case from previous step of existing Dynamic Contingency Analysis

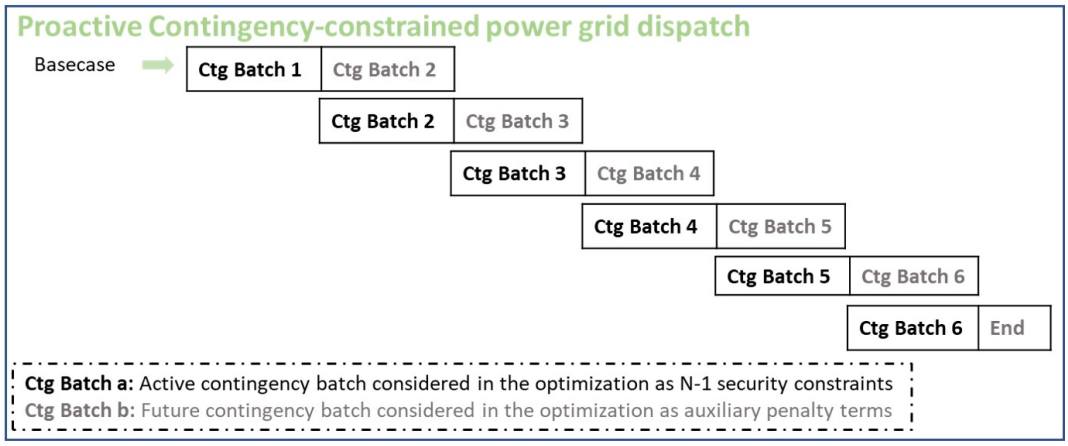

Figure 3.1: An illustration of multi-step cascaded optimization considering hurricane progression.

Toolbox (DCAT) simulation can be utilized in next step, as a new operation basecase. Then contingency list will be updated for individual step, as hurricane will continue to move through the power grid spanning over large geographical areas.

It should be noted that with the predictive intelligence derived from hurricane modeling, one potential idea would be for one hurricane step, not only using the contingencies in the current step list, but also imposing further constraints on transmission line yet to-be-impacted in next step, i.e., more conservative constraints of line flow ratings (100% to 70%); therefore, the resulted contingency-constrained SCOPF problem is further extended with proactive posturing capability throughout the hurricane life cycle. Fig. 3.1 provides an illustrative example with 6 steps representing one historical hurricane.

3.3 NUMERICAL RESULTS

To evaluate and validate our proposed methodology, a real-world power grid model is utilized considering a single historical hurricane event. The power system model considered is a 1263-Bus and 1269-Branch network [55]. Based on historical hurricane event data in 2017, one realization of the hurricane was derived considering wind speed variations.

Moreover, within this realization the hurricane process is divided into six consecutive steps; each step is a set of power system contingencies, such as credible transmission line, bus and generator outages along the hurricane trajectory shown in Table 3.1. Detailed examples and illustrations can be found in *Section 5, Simulation Results* in [55].

Simulations are performed on a laptop with an Intel Core i5 2.3 GHz CPU and 8 GB RAM using MATLAB R2020b. The open-source solver SDPT3 is used to solve the semidefinite program through CVX v2.1 [45]. The objective function for each contingency batch is the sum of operation cost over time scale of 15 minutes as each contingency (Ctg) batch from DCAT has the same time scale. For each step in the hurricane progression, grid data obtained through DCAT is fed as a basecase to the optimization problem. The output of the optimization is then analyzed. This multi-step cascaded optimization setup is illustrated in Figure 3.1.

Table 3.1: Contingency Data and Operation Cost

Contingency Batches	# of Buses Lost	# of Branches Lost	# of Generators Lost	Operation Cost ($)
Ctg Batch 1	0	0	0	99,638
Ctg Batch 2	0	1	0	114,248
Ctg Batch 3	90	114	2	–
Ctg Batch 4	268	318	4	1,537,810
Ctg Batch 5	376	447	5	–
Ctg Batch 6	401	481	5	–

3.3.1 Operation Cost

In the simulations, the optimizer found an optimal solution to the SDP relaxation after computation time of 2 minutes 46 seconds. It was observed that the cost of operating the grid during hurricane-triggered contingencies gradually increases as the hurricane progresses through the grid network and causes loss to network elements. This result is shown in Ta-

ble 3.1, operation cost gradually increases from a basecase cost of $99,638 to $1,537,810 in Ctg Batch 4. This can be attributed to increased utilization of network elements as a result of the loss of buses, branches and generators in the network making the electric grid more and more expensive to operate. In Ctg Batch 3, 5, and 6 the model becomes infeasible due to the grids inability to survive outage to several damaged elements.

3.3.2 Proactive Mitigation Measure

Hurricane impacts which lead to fatal damage to grid elements such as lines, buses, generators, transformer etc. can be mitigated by applying proactive measures to adjust their operation during hurricane progression while still maintaining reliability to serve as many customers as possible. To test proactive measures, We apply tighter line flow constraints to Ctg Batch branches to power flow cases generated through DCAT's time domain simulation. In the experiments, line flows on branches in the hurricane's path are proactively limited to operate at 70% of normal operation limits.

In Figure 3.2, we observe that line flows over branch #77 reduces by a maximum of 7% when we applying a proactive mitigation strategy of tightening branch flow constraints without violating other constraints or the optimization model becoming infeasible.We can further tighten the line flow limits below 70% until we reach infeasibility of the model for the purpose of analysis; additional runs with progressively tighter branch flow constraints indicated that the model becomes infeasible when line flow limits fall below 40% of normal operation while still meeting the system load demand.

3.4 CONCLUSIONS

The paper aims to develop interactive cross-domain data analytics based on hurricane modeling, power system optimization and model-based simulations. The temporal relations among individual steps (groups of time period) within historical hurricane event have been

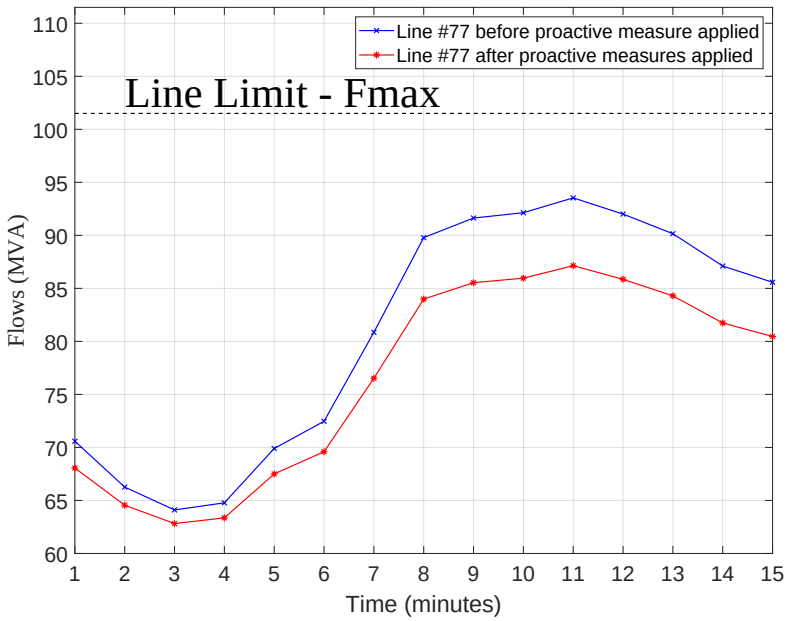

Figure 3.2: Line MVA flows on line # 77 before and after applying proactive mitigation to penalize the flow on selected lines in the hurricane path

explored and transformed into explicit optimization constraints, and further incorporated into SCOPF problem to identify proactive posturing of power system elements. Variations of the operation cost among different hurricane steps (contingency batches) indicates the applicability of such optimization formulation, and the improvement in targeted credible line contingencies shows promising improvements by such proactive dispatch. Future work includes scalability evaluation with large volume of DCAT simulation outputs based on different base cases and synthesized hurricane events, and expanded validation considering multiple resilience metrics [55].

CHAPTER 4

MICROGRID SCHEDULING WITH UNCERTAINTY IN TRANSIENT LOAD

Microgrid Scheduling with Uncertainty in Transient Load[1]

E. Quarm Jnr. and R. Madani. "Microgrid Scheduling with Uncertainty Transient Load "

– In preparation for publication.

[1]Copyright © Reprinted, with permission, from R. Madani, Microgrid Scheduling with Uncertainty Transient Load.

Microgrid Scheduling under Uncertainty Transient Load

Edward Quarm Jnr. and Ramtin Madani

The authors are with the Department of Electrical Engineering, University of Texas at Arlington (email: edwardarthur.quarmjnr@uta.edu, ramtin.madani@uta.edu)

Abstract — Microgrids (MGs) have the potential to increase grid reliability by alleviating burden on the main grid. However due to the lack of adequate reserve margins, imbalances between demand and supply become problematic in island mode making the MG prone to collapse. In this paper, we formulate the MG scheduling problem which considers uncertainty introduced by transient load demand. A convex relaxation is formulated which is capable of finding feasible solutions within a provable distance from global optimality. We demonstrate the performance of this approach on a modified IEEE 14-bus and compare to numerical solvers and other methods of relaxation. Through experiments, we demonstrate that Energy Storage Units (ESUs) have the potential to enhance MG reliability even in the presence of highly variable transient load demand. The analysis performed in this paper can serve as a guide to MG operators to determine ESU size needed to achieve a desired load profile in a scheduling problem under uncertainty. Additionally, we demonstrate that the proposed convex relaxation is able to tackle the MG scheduling problem under uncertainty without a need to occasionally adopt scenario reduction methods when MIP solvers are utilized.

Keywords — Microgrid security, Energy Storage, Optimization methods.

4.1 INTRODUCTION

Microgrids (MGs) have gained importance as a reliable way to alleviate the burden on the main grid and provide the needed resiliency required in today's power system. This interest has led to investment and research into operations, control, planning and design of the technology [75]. Even as the grid goes through radical changes, the MG technology will need further improvement in order to make way for a resilient futuristic grid.

MGs are an important piece of the grid infrastructure because they enhance grid resilience, help reduce grid disturbance and function as a grid resource for faster system response and recovery [76]. In addition, they reduce carbon emissions thereby helping to preserve the environment. Typical MG infrastructure consists of Distributed Generators (DGs), Energy Storage Units (ESUs) and Renewable Energy Resources (RES) like photovoltaic, wind and in certain cases biomass generators. ESUs make MGs sustainable as they coordinate with DGs to guarantee generation adequacy and also smoothen out load imbalances . During grid interruption, ESUs can serve as a load balancing and translational source while back-up generators are given time to kick in [77].

The MG scheduling problem is an essential piece to the autonomous operation and control of the technology. This problem aims to determine the optimal schedule of DGs to meet forecasted demand while satisfying technological and operational constraints of the MG. The resulting commitment decisions are implemented by centralized, decentralized or hierarchical controllers that also communicate with the main grid depending on the system architecture [78–81].

One major issue with operating MGs autonomously is their lack of adequate reserve margins and rotating inertia of synchronous generators that the main grid possess which enforce demand-supply equilibrium and dampen out grid transients. While in grid-connected mode, MGs rely on power exchanges with the main grid to mitigate steep load demand variations. However, in island mode it is difficult to alleviate this mismatch because of the

slow ramp response and inadequate reserve margins of DGs. These phenomena contributes to voltage and frequency dips, increase the cost and reduce the fuel efficiency of DG power supply due to operation of DGs at low capacity factors [82]. One way to handle this is to ensure constant energy exchange with the macrogrid and demand side management strategies such as load shedding as proposed in [83, 84] respectively, however the two options are not always achievable or desirable in island mode.

A variety of methods have been proposed in literature to tackle the MG scheduling problem, however only a few consider the effect of load demand uncertainty on MG security. For instance, authors in [85] formulated a two-stage stochastic mixed-integer MG scheduling problem with RES being the only source of uncertainty. In [86], uncertainties namely wind speed, day-ahead market price and MG load were considered in using a two-stage stochastic formulation. Power generation schedules without uncertainties were determined in the first stage, and feasible schedules due to uncertain variables determined in the second stage. In [87] the authors made an attempt to consider both intermittency of RES and demand in the problem formulation, using a probability-based index to describe the uncertainties rather than scenario probability density functions which will be utilized in this paper.

Operating the MG in island mode presents many challenges to reliability of generation to meet load demand. Islanding constraints were introduced for the purpose of enhancing resiliency in MGs in [88, 89]. To enforce MG security, scheduling decisions were revised using islanding cuts if sufficient generation is not available to guarantee a feasible islanding in [88]. Load curtailment has been explored as an option to ensure adequate generation to supply demand [84, 90] although this method is generally undesirable for consumers.

MG scheduling problems easily becomes intractable to be solved by Mixed-Integer Programming (MIP) solver when more scenarios are considered. To resolve this problem

[91] suggest trimming down scenarios. Scenario reduction techniques were also applied in [92] to trim the large number of wind and photovoltaic scenarios generated by Monte Carlo sampling to be solved by CPLEX. The authors in [93] realized the need to consider the uncertainties in both supply and demand, however the problem was formulated as a trajectory tracking problem using Stochastic Model Predictive Controller (SMPC).

Uncertainty of RES in MG has been modeled using the method of chance-constrained programming [83,89]. In [83] chance-constrained optimization was used to minimize operational cost of MG and to ensure energy exchange commitments between MG and macrogrid were met. In [94] spinning reserves requirements were considered in order to compensate for load variations during the island mode. However with this approach the total generation cost becomes larger due to the additional reserve and besides doesn't alleviate the sharp dips and ramps of DGs.

The contributions of this paper are in three-fold: I. We present a stochastic MG scheduling problem which considers load demand uncertainty in the form of transient load and DG outage contingencies in the formulation. II. We propose a scalable method based on convex relaxations to solve the stochastic MG scheduling formulation under uncertainty. III. We present simulation results showing improvement to MG security. The scheduling strategy is to utilize ESUs to improve load profile in island mode while minimizing operational costs of the MG.

A high number of uncertain scenarios and system contingencies increases problem size and hence makes the MIP formulation intractable to be solved by MIP solvers [86, 91, 92], hence we leverage the power of SDP relaxation to alleviate the burden of branch-and-bound search. While off-the-shelf SDP relaxation produces a lower bound on the optimal objective, it is computationally prohibitive thus not scalable [35, 36]. Hence, in this work, we are forging a low-complexity conic relaxation that is capable of solving detailed MG scheduling. This effort is aligned with the recent body of research devoted

to scalable variants of semidefinite programming [37]. In lieu of computationally demanding constraints, we employ low-order SDP constraints to determine binary variables. So as to strengthen the relaxation, valid inequalities are introduced from the multiplication of constraints through the Reformulation-Linearization Technique (RLT). To address cases for which the proposed relaxation is not exact, we propose a heuristic approach to infer near-globally optimal points from the outcome of convex relaxation.

The remainder of this paper is organized as follows. In Section 4.2.2, we formulate the MG scheduling problem under uncertainty. This non-convex problem is convexified by means of convex surrogates in Section 4.3. Next, a scalable convex relaxation is proposed in Section 4.3 to tackle MG scheduling in polynomial time. Section 4.4 proposes a heuristic approach to infer near-globally optimal points from the outcome of convex relaxation. Extensive experiments are presented in Section 4.5. Section 4.6 concludes the paper.

4.1.1 Notations

Throughout this paper, matrices, vectors and scalars are represented by boldface uppercase, boldface lowercase and italic lowercase letters, respectively. $|\cdot|$ represents the absolute value of a scalar or the cardinality of a set. The symbol $(\cdot)^\top$ represents the transpose operator. Given a matrix $\boldsymbol{A}$, the notation $\boldsymbol{A}_{jk}$ refers to its $(j,k)^{th}$ element. $\boldsymbol{A} \succeq 0$ means that $\boldsymbol{A}$ is symmetric and positive semidefinite.

4.2 MG SCHEDULING PROBLEM

This work considers the MG scheduling problem under load demand uncertainty. Furthermore, we consider contingencies arising from DG outages in the formulation. We employ a stochastic approach to modeling security motivated by [34] and MATPOWER Optimal Scheduling software package. This involves defining re-dispatch variables in the problem

formulation which represents recourse decisions contingent on the outcome of an uncertainty.

4.2.1 Multi-scenario Load demand Profile

Load demand is a major source of uncertainty in an MG. Typically, load uncertainty is introduced by forecasting errors and consumer decision on energy usage [85,91,92]. Proposing algorithms to handle uncertainty becomes even more challenging when transient load demand is considered in the formulation. In this paper, uncertainty is modeled as scenarios with continuous probability distributions where each scenario represents a different realization of load demand with an assigned probability of occurrence. In order to model uncertainty in demand, we define a transition probability matrix to describe transitions the set of base scenarios in one period to the set of base scenarios in the next period.

Figure 4.1 shows three types of demand profiles used to build scenarios. They include:

4.2.1.1 Base Loads

Base loads represent the minimum predicted load demand profile at constant magnitude over the time horizon.

4.2.1.2 Peak Loads

Peak loads represent the maximum predicted load demand profile at constant magnitude over the time horizon.

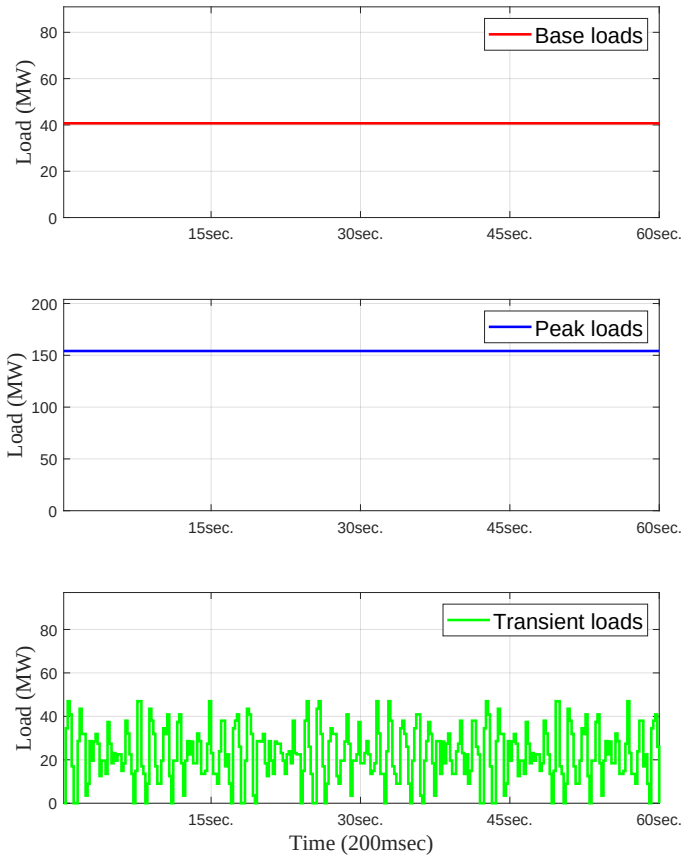

Figure 4.1: Load demand profiles. First from top: group 1 - Base loads. Second from top: group 2 - Peak loads. Third from top - Transient loads.

4.2.1.3 Transient Loads

Transient loads represent predicted load demand profile with pulsating behavior over the time horizon.

4.2.2 Problem Formulation

The Microgrid (MG) scheduling problem aims to find the optimal schedule of Distributed Generators (DGs) and Energy Storage Units (ESU) throughout a discrete time horizon $\mathcal{T}$, subject to demand forecast and operational constraints.

4.2.3 Objective function

The objective of MG scheduling problem is to minimize the expected value of the total cost throughout the time horizon $\mathcal{T}$, and across the set of scenarios and contingencies. This objective is made up of the expected base case and post-contingency generation costs, ramping "wear and tear" costs, load-following ramp reserve and contingency reserve costs, as well as the generator start-up, shutdown and fixed costs. This objective function can be cast with respect to the following three expressions:

$$\sum_{t\in\mathcal{T}} \gamma_t \sum_{g\in\mathcal{G}_t} \sigma_{tg}^{(1)}(x_{tg}, r_{tg}^{+}, r_{tg}^{-}, w_{tg}^{+}, w_{tg}^{-}) \tag{4.1a}$$

$$\sum_{t\in\mathcal{T}} \sum_{s\in\mathcal{S}_t} \sum_{c\in\mathcal{C}_{ts}} \psi_{tsc} \sum_{g\in\mathcal{G}_{tsc}} \sigma_{tg}^{(2)}(p_{tgsc}, p_{tg}^{\text{ref}}) \tag{4.1b}$$

$$\sum_{t\in\mathcal{T}} \gamma_t \sum_{s_1\in\mathcal{S}_{t-1}} \sum_{s_2\in\mathcal{S}_t} \phi_{ts_1s_2} \sum_{g\in\mathcal{G}_{ts_20}} \sigma_g^{(3)}(p_{tgs_20}, p_{(t-1)gs_10}) \tag{4.1c}$$

In the first line of the objective (4.1a), the cost function $\sigma_{tg}^{(1)}$is defined as

$$\sigma_{tg}^{(1)}(x_{tg}, r_{tg}^{+}, r_{tg}^{-}, w_{tg}^{+}, w_{tg}^{-}) \triangleq \zeta_{tg}\, x_{tg} \tag{4.2a}$$

$$+ \zeta_{tg}^{\uparrow}\, (1 - x_{(t-1)g}) x_{tg} \tag{4.2b}$$

$$+ \zeta_{tg}^{\downarrow}\, x_{(t-1)g}(1 - x_{tg}) \tag{4.2c}$$

$$+ (\eta_{tg}^{+}\, r_{tg}^{+} + \eta_{tg}^{-}\, r_{tg}^{-}) \tag{4.2d}$$

$$+ (\mu_{tg}^{+}\, w_{tg}^{+} + \mu_{tg}^{-}\, w_{tg}^{-}) \tag{4.2e}$$

with the expressions (4.2a), (4.2b) and (4.2c) corresponding to generator fixed, startup and shutdown costs, respectively; while (4.2d) and (4.2e) account for the cost of contingency and load-following ramping reserves, respectively.

In the second line (4.1b), the function $\sigma^{(2)}_{tg}(\cdot,\cdot)$ is defined as

$$\sigma^{(2)}_{tg}(p_{tgsc}, p^{\text{ref}}_{tg}) \triangleq \alpha^{\text{sqr}}_{tg}\ p^2_{tgsc} + \alpha^{\text{lin}}_{tg}\ p_{tgsc} + \tag{4.3a}$$

$$\frac{\beta^+_{tg}+\beta^-_{tg}}{2}\,|\,p_{tgsc}-p^{\text{ref}}_{tg}|+\frac{\beta^+_{tg}-\beta^-_{tg}}{2}(p_{tgsc}-p^{\text{ref}}_{tg}) \tag{4.3b}$$

including the quadratic expression (4.3a) with nonnegative quadratic and linear coefficients α^{sqr}_{tg} and α^{lin}_{tg}, and the term (4.3b) for assigning costs to deviations from reference values with nonnegative coefficients β^+_{tg} and β^-_{tg}. These costs are weighted by the probability of contingency ψ_{tsc}.

Finally, we have the third term (4.1c), we have the term representing a quadratic load-following ramp "wear and tear" cost

$$\sigma^{(3)}_{g}(p_{tgs_20}, p_{(t-1)gs_10}) \triangleq \kappa_g \times (p_{tgs_20} - p_{(t-1)gs_10})^2 \tag{4.4}$$

weighted by γ_t, the nonnegative coefficients κ_g, and $\phi_{ts_1s_2}$.

4.2.4 Constraints

We apply the following constraints to the MG scheduling problem for every $t \in \mathcal{T}$ and $g \in \mathcal{G}_t$:

$$x_{tg} \in \{0,1\} \tag{4.5}$$

$$\underline{p}_g\ x_{tg} \le p_{tgsc} \le \bar{p}_g\ x_{tg} \qquad \forall s \in \mathcal{S}_t,\ \forall c \in \mathcal{C}_{ts} \tag{4.6}$$

$$x_{tg} \ge x_{\tau g} - x_{(\tau-1)g} \qquad \forall \tau \in \{t - m^{\uparrow}_g + 1, \ldots, t\} \tag{4.7}$$

$$1 - x_{tg} \ge x_{(\tau-1)g} - x_{\tau g} \qquad \forall \tau \in \{t - m^{\downarrow}_g + 1, \ldots, t\} \tag{4.8}$$

$$0 \le w^+_{tg} \le \bar{w}_{tg}, \tag{4.9}$$

$$0 \leq w^{-}_{tg} \leq \underline{w}_{tg}, \tag{4.10}$$

$$p_{tgs_20} - p_{(t-1)gs_10} \leq w^{+}_{(t-1)g}, \quad \forall s_1 \in \mathcal{S}_{t-1},\ \forall s_2 \in \mathcal{S}_t \tag{4.11}$$

$$p_{(t-1)gs_10} - p_{tgs_20} \leq w^{-}_{(t-1)g}, \quad \forall s_1 \in \mathcal{S}_{t-1},\ \forall s_2 \in \mathcal{S}_t \tag{4.12}$$

$$0 \leq r^{+}_{tg} \leq \bar{r}_{tg}, \tag{4.13}$$

$$0 \leq r^{-}_{tg} \leq \underline{r}_{tg}, \tag{4.14}$$

$$p_{tgsc} - p^{\text{ref}}_{tg} \leq r^{+}_{tg}, \quad \forall s \in \mathcal{S}_t,\ \forall c \in \mathcal{C}_{ts} \tag{4.15}$$

$$E^{+}_{tg} \leq \bar{E}_g, \tag{4.16}$$

$$\underline{E}_g \leq E^{-}_{tg}, \tag{4.17}$$

$$\underline{E}_g \leq E^{-}_{(t-1)g} + E^{\Delta}_{tgsc}, \quad \forall s \in \mathcal{S}_t,\ \forall c \in \mathcal{C}_{ts} \tag{4.18}$$

$$E^{+}_{(t-1)g} + E^{\Delta}_{tgsc} \leq \bar{E}_g, \quad \forall s \in \mathcal{S}_t,\ \forall c \in \mathcal{C}_{ts} \tag{4.19}$$

$$E^{\Delta}_{tgsc} \triangleq -\Delta(\rho^{\text{in}}_g p^{\text{ESU+}}_{tgsc} + \frac{1}{\rho^{\text{out}}_g} p^{\text{ESU-}}_{tgsc}), \quad \forall s \in \mathcal{S}_t,\ \forall c \in \mathcal{C}_{ts} \tag{4.20}$$

$$p^{\text{ref}}_{tg} - p_{tgsc} \leq r^{-}_{tg}, \quad \forall s \in \mathcal{S}_t,\ \forall c \in \mathcal{C}_{ts} \tag{4.21}$$

$$-\underline{\Delta}_g \leq p_{tgsc} - p_{tgs0} \leq \bar{\Delta}_g, \quad \forall s \in \mathcal{S}_t,\ \forall c \in \mathcal{C}_{ts} \tag{4.22}$$

$$p_{tgsc} = p^{\text{ESU+}}_{tgsc} + p^{\text{ESU-}}_{tgsc}, \quad \forall s \in \mathcal{S}_t,\ \forall c \in \mathcal{C}_{ts} \tag{4.23}$$

$$p^{\text{ESU+}}_{tgsc} \leq 0, \quad \forall s \in \mathcal{S}_t,\ \forall c \in \mathcal{C}_{ts} \tag{4.24}$$

$$0 \leq p^{\text{ESU-}}_{tgsc}, \quad \forall s \in \mathcal{S}_t,\ \forall c \in \mathcal{C}_{ts} \tag{4.25}$$

$$E^{-}_{tg} \leq E^{-}_{(t-1)g} + E^{\Delta}_{tgs0} - \Delta\frac{\rho^{\text{loss}}_{g}}{2}(E^{-}_{tg} + E^{-}_{(t-1)g}),$$

$$\forall s \in \mathcal{S}_t,\ \forall c \in \mathcal{C}_{ts} \tag{4.26}$$

$$\Delta\frac{\rho^{\text{loss}}_{g}}{2}(E^{+}_{tg} + E^{+}_{(t-1)g}) - E^{+}_{(t-1)g} - E^{\Delta}_{tgs0} \leq E^{+}_{tg},$$

$$\forall s \in \mathcal{S}_t,\ \forall c \in \mathcal{C}_{ts} \tag{4.27}$$

$$\sum \boldsymbol{p}_{tsc} = \sum \boldsymbol{d}_{tsc}, \qquad \forall s \in \mathcal{S}_t,\ \forall c \in \mathcal{C}_{ts} \tag{4.28}$$

where

$$\boldsymbol{p}_{tsc} \triangleq \left[p_{t1sc},\ p_{t2sc},\ \ldots,\ p_{t|\mathcal{G}_{tsc}|sc}\right]^{\top} \tag{4.29}$$

Constraint (4.5) imposes binary requirements on units in the MG. Upper and lower limits $\{\underline{p}_{tgsc}\ ,\ \bar{p}_{tgsc}\}$ on DG active power injections are imposed by the constraint (4.6). The DG units are subject to minimum up and down time limits in (4.7) – (4.8). Per-period ramp limits are imposed on the units with constraints (4.9) – (4.12). Constraints (4.13) – (4.15) – (4.21) impose upward/downward limits $\{\bar{r}_{tg}\ ,\ \underline{r}_{tg}\}$ on post-contingency dispatch quantities, respectively. Additionally, constraint (4.22) enforces limits on downward and upward transitions from base to post-contigency cases.

ESU constraints (4.23) – (4.25) and (4.16) – (4.17) impose charging and discharging limits $\{\underline{p}_{tgsc},\ \bar{p}_{tgsc}\}$ and energy limits $\{\underline{E}_g,\ \bar{E}_g\}$ on storage units, respectively. Constraint (4.18) – (4.19) represent the amount of energy stored in a given unit in post-contingency state at the end of period t. Furthermore, constraints (4.26) – (4.27) represents the amount of energy stored in storage unit in basecase at the end of period t. Constraint (4.28) imposes the balance between DG power generation $\boldsymbol{p}_{tsc}$ and uncertain load demand $\boldsymbol{d}_{tsc} \in \mathbb{R}$.

Given the above three-part expression in (4.1) and constraints in (4.5) – (4.28), the Stochastic MG scheduling problem can be formulated as the optimization:

$$\begin{aligned}
&\text{minimize} && \text{(4.1a)+(4.1b)+(4.1c)} && && \text{(4.30a)}\\
&\text{subject to} && \text{(4.5)} - \text{(4.27)} && \forall t \in \mathcal{T},\ \ \forall g \in \mathcal{G}_t && \text{(4.30b)}\\
& && \text{(4.28)} && \forall t \in \mathcal{T} && \text{(4.30c)}
\end{aligned}$$

with respect to variables $\{x_{tg}\}$, $\{p_{tgsc}\}$, $\{p^{+\mathrm{ESU}}_{tgsc}\}$, $\{p^{-\mathrm{ESU}}_{tgsc}\}$, $\{p^{\mathrm{ref}}_{tg}\}$, $\{r^{+}_{tg}\}$, $\{r^{-}_{tg}\}$, $\{w^{+}_{tg}\}$, $\{w^{-}_{tg}\}$, $\{E^{-}_{tg}\}$ and $\{E^{-}_{tg}\}$.

4.3 CONVEXIFICATION OF MG SCHEDULING PROBLEM

In this section, we construct convex relaxations in order to efficiently tackle the MG scheduling problem (2.12). We employ conic relaxations combined with a set of valid inequalities which lead to a computationally-tractable convex formulation. To this end, we transition to a lifted space by introducing additional auxiliary variables each accounting for a quadratic monomial. We then formulate a SOCP relaxation based on the "perspective relaxation" in [39]. Finally, a strong SDP relaxation is formulated using additional variables and valid inequalities.

4.3.1 Lifted objective

To formulate convex relaxations we first lift the objective function (2.1) into a higher-dimensional space in which it is piecewise linear. This is done by introducing the variables

$$\begin{aligned}
&\big\{u_{tg}\big\}_{t\in\mathcal{T},\, g\in\mathcal{G}_t},\quad \big\{h_{tgs_1s_2}\big\}_{t\in\mathcal{T},\, g\in\mathcal{G}_t,\, s_1\in\mathcal{S}_{t-1},\, s_2\in\mathcal{S}_t},\\
&\big\{o_{tgsc}\big\}_{t\in\mathcal{T},\, g\in\mathcal{G}_t,\, s\in\mathcal{S}_t,\, c\in\mathcal{C}_{ts}}
\end{aligned}$$

representing the products

$$\{x_{(t-1)g}\, x_{tg}\}, \quad \{p_{(t-1)gs_10} \times p_{tgs_20}\}, \quad \{p^2_{tgsc}\} \tag{4.31}$$

respectively. Consider the following lifted objective function components:

$$\sum_{t\in\mathcal{T}} \gamma_t \sum_{g\in\mathcal{G}_t} \bar{\sigma}^{(1)}_{tg}(x_{tg}, u_{tg}, r^+_{tg}, r^-_{tg}, w^+_{tg}, w^-_{tg}) \tag{4.32a}$$

$$\sum_{t\in\mathcal{T}} \sum_{s\in\mathcal{S}_t} \sum_{c\in\mathcal{C}_{ts}} \psi_{tsc} \sum_{g\in\mathcal{G}_{tsc}} \bar{\sigma}^{(2)}_{tg}(p_{tgsc}, o_{tgsc}, p^{\text{ref}}_{tg}) \tag{4.32b}$$

$$\sum_{t\in\mathcal{T}} \gamma_t \sum_{s_1\in\mathcal{S}_{t-1}} \sum_{s_2\in\mathcal{S}_t} \phi_{ts_1s_2} \sum_{g\in\mathcal{G}_{ts_20}} \bar{\sigma}^{(3)}_{g}(o_{tgs_20}, o_{(t-1)gs_10}, h_{tgs_2s_1}) \tag{4.32c}$$

where for each $t \in \mathcal{T}$ and $g \in \mathcal{G}_t$

$$\bar{\sigma}^{(1)}_{tg}(x_{tg}, u_{tg}, r^+_{tg}, r^-_{tg}, w^+_{tg}, w^-_{tg}) \triangleq \zeta_{tg}\; x_{tg} \tag{4.33a}$$

$$+ \zeta^{\uparrow}_{tg}\; (x_{tg} - u_{tg}) \tag{4.33b}$$

$$+ \zeta^{\downarrow}_{tg}\; (x_{(t-1)g} - u_{tg}) \tag{4.33c}$$

$$+ (\eta^+_{tg}\; r^+_{tg} + \eta^-_{tg}\; r^-_{tg}) \tag{4.33d}$$

$$+ (\mu^+_{tg}\; w^+_{tg} + \mu^-_{tg}\; w^-_{tg}) \tag{4.33e}$$

encapsulates the lifted startup and shutdown costs and

$$\bar{\sigma}^{(2)}_{tg}(p_{tgsc}, o_{tgsc}, p^{\text{ref}}_{tg}) \triangleq \alpha^{\text{sqr}}_{tg}\; o_{tgsc} + \alpha^{\text{lin}}_{tg}\; p_{tgsc} + \tag{4.34a}$$

$$\frac{\beta^+_{tg}+\beta^-_{tg}}{2}\,|\,p_{tgsc}-p^{\text{ref}}_{tg}|+\frac{\beta^+_{tg}-\beta^-_{tg}}{2}(p_{tgsc}-p^{\text{ref}}_{tg}). \tag{4.34b}$$

represents the lifted quadratic cost function. Additionally, for each $g \in \mathcal{G}$,

$$\bar{\sigma}_g^{(3)}(o_{tgs_20}, o_{(t-1)gs_10}, h_{tgs_1s_2}) \triangleq \\ \kappa_g \times (o_{tgs_20} + o_{(t-1)gs_10} - 2h_{tgs_1s_2}) \tag{4.35}$$

is the lifted "wear and tear" cost.

4.3.2 LP and perspective relaxations

For every $t \in \mathcal{T}$ and $g \in \mathcal{G}_t$, the relation between the auxiliary variables $\{u_{tg}\}$ and their corresponding monomials can be enforced using the following valid inequalities:

$$\max\{0,\ x_{(t-1)g} + x_{tg} - 1\} \leq u_{tg} \leq \min\{x_{(t-1)g}, x_{tg}\} \tag{4.36}$$

The role of (4.36) is to ensure that the lifted costs (2.14a) is equivalent to the original costs (2.1a). Through simple enumeration of the set $(x_{g(t-1)}, x_{gt}) \in \{0,1\}^2$, it can be observed that

$$(4.5) \wedge (4.36) \quad \Rightarrow \quad u_{tg} = x_{tg} x_{(t-1)g}$$

, for every $t \in \mathcal{T}$ and $g \in \mathcal{G}_t$.

Lifting the first part of the objective and the transformation of $x_{gt} \in \{0,1\}$ to $0 \leq x_{tg} \leq 1$, results in the following LP relaxation of the MG scheduling problem [40–42]:

minimize	(2.14a)+(2.1b)+(2.1c)		(4.37a)
subject to	$0 \leq x_{tg} \leq 1$	$\forall t \in \mathcal{T},\ \forall g \in \mathcal{G}_t$	(4.37b)
	(2.6)–(4.27), (4.36)	$\forall t \in \mathcal{T},\ \forall g \in \mathcal{G}_t$	(4.37c)
	(2.10a)	$\forall t \in \mathcal{T}$	(4.37d)

As shown in [39], the performance of this approach can be significantly improved by lifting (2.1b) to (2.14b), and relaxing $o_{tgsc} = p_{tgsc}^2$ to the SOCP and McCormick constraint

$$o_{tgsc}\, x_{tg} \geq p_{tgsc}^2, \quad o_{tgsc} \geq 0 \qquad \forall s \in \mathcal{S}_t,\ \forall c \in \mathcal{C}_{ts} \tag{4.38a}$$

$$o_{tgsc} + \underline{p}_g\, \bar{p}_g\, x_{tg} \leq (\underline{p}_g + \bar{p}_g) p_{tgsc} \qquad \forall s \in \mathcal{S}_t,\ \forall c \in \mathcal{C}_{ts} \tag{4.38b}$$

which results in the following perspective relaxation:

minimize	(2.14a)+(2.14b)+(2.1c)		(4.39a)
subject to	$0 \leq x_{tg} \leq 1$	$\forall t \in \mathcal{T},\ \forall g \in \mathcal{G}_t$	(4.39b)
	(2.6)–(4.27), (4.36), (4.38)	$\forall t \in \mathcal{T},\ \forall g \in \mathcal{G}_t$	(4.39c)
	(2.10a)	$\forall t \in \mathcal{T}$	(4.39d)

In the remainder of this section, we will construct an SDP relaxation as an alternative to (4.39).

$$\begin{bmatrix} x_{(t-1)g} & * & * & * & * \\ u_{tg} & x_{tg} & * & * & * \\ u_{tg} & u_{tg} & u_{tg} & * & * \\ p_{(t-1)gs_10} & z_{tgs_1} & z_{tgs_1} & o_{(t-1)gs_10} & * \\ y_{tgs_1} & p_{tgs_20} & y_{tgs_1} & h_{tgs_1s_2} & o_{tgs_20} \end{bmatrix} \succeq 0 \qquad \forall s_1 \in \mathcal{S}_{t-1},\ \forall s_2 \in \mathcal{S}_t \tag{4.40a}$$

$$\underline{p}_g \left(p_{tgs_10} + p_{tgs_20}\right) \ \leq \ h_{tgs_1s_2} + \underline{p}_g^2 \, u_{tg} \qquad \forall s_1 \in \mathcal{S}_{t-1},\ \forall s_2 \in \mathcal{S}_t \tag{4.40b}$$

$$\bar{p}_g \left(p_{tgs_10} + p_{tgs_20}\right) \ \leq \ h_{tgs_1s_2} + \bar{p}_g^2 \, u_{tg} \qquad \forall s_1 \in \mathcal{S}_{t-1},\ \forall s_2 \in \mathcal{S}_t \tag{4.40c}$$

$$h_{tgs_1s_2} + \underline{p}_g \bar{p}_g \, u_{tg} \ \leq \ \bar{p}_g \, y_{tgs_1} + \underline{p}_g \, z_{tgs_1} \qquad \forall s_1 \in \mathcal{S}_{t-1},\ \forall s_2 \in \mathcal{S}_t \tag{4.40d}$$

$$h_{tgs_1s_2} + \underline{p}_g \bar{p}_g \, u_{tg} \ \leq \ \underline{p}_g \, y_{tgs_1} + \bar{p}_g \, z_{tgs_1} \qquad \forall s_1 \in \mathcal{S}_{t-1},\ \forall s_2 \in \mathcal{S}_t \tag{4.40e}$$

$$\underline{p}_g \, u_{tg} \ \leq \ y_{tgs_1} \ \leq \ \bar{p}_g \, u_{tg} \qquad \forall s \in \mathcal{S}_t \tag{4.40f}$$

$$\underline{p}_g \, u_{tg} \ \leq \ z_{tgs_1} \ \leq \ \bar{p}_g \, u_{tg} \qquad \forall s \in \mathcal{S}_t \tag{4.40g}$$

$$\bar{p}_g \left(u_{tg} - \, x_{tg}\right) \quad \leq \ y_{tgs_1} - p_{tgs0} \quad \leq \ \underline{p}_g \left(u_{tg} - \, x_{tg}\right) \qquad \forall s \in \mathcal{S}_t \tag{4.40h}$$

$$\bar{p}_g \left(u_{tg} - \, x_{(t-1)g}\right) \ \leq \ z_{tgs_1} - p_{(t-1)gs0} \ \leq \ \underline{p}_g \left(u_{tg} - \, x_{(t-1)g}\right) \qquad \forall s \in \mathcal{S}_t \tag{4.40i}$$

4.3.3 SDP relaxation

To forge a stronger relaxation, consider the new variables

$$\left\{z_{tgs}\right\}_{t \in \mathcal{T},\, g \in \mathcal{G}_t,\, s \in \mathcal{S}_t}, \qquad \left\{y_{tgs}\right\}_{t \in \mathcal{T},\, g \in \mathcal{G}_t,\, s \in \mathcal{S}_t}$$

representing monomials $\{p_{(t-1)gs0}x_{tg}\}$ and $\{p_{tgs0}x_{(t-1)g}\}$, respectively. In place of (4.37b), we impose a collection of conic and linear inequalities (4.40), resulting in the following SDP relaxation of SCUC:

$$\begin{aligned}
&\text{minimize} && \text{(2.14a)+(2.14b)+(2.14c)} && && \text{(4.41a)}\\
&\text{subject to} && \text{(4.40)} && \forall t \in \mathcal{T},\ \forall g \in \mathcal{G}_t && \text{(4.41b)}\\
& && \text{(2.6)}-\text{(4.27), (4.36), (4.38)} && \forall t \in \mathcal{T},\ \forall g \in \mathcal{G}_t && \text{(4.41c)}\\
& && \text{(2.10a)} && \forall t \in \mathcal{T} && \text{(4.41d)}
\end{aligned}$$

The matrix inequality (4.40a) is a surrogate for:

$$\begin{bmatrix}
x_{(t-1)g} & * & * & * & *\\
u_{tg} & x_{tg} & * & * & *\\
u_{tg} & u_{tg} & u_{tg} & * & *\\
p_{(t-1)gs_10} & z_{tgs_1} & z_{tgs_1} & o_{(t-1)gs_10} & *\\
y_{tgs_1} & p_{tgs_20} & y_{tgs_1} & h_{tgs_1s_2} & o_{tgs_20}
\end{bmatrix} = \begin{bmatrix} x_{(t-1)g}\\ x_{tg}\\ u_{tg}\\ p_{(t-1)gs_10}\\ p_{tgs_10}\end{bmatrix}\begin{bmatrix} x_{(t-1)g} & x_{tg} & u_{tg} & p_{(t-1)gs_10} & p_{tgs_10}\end{bmatrix} \tag{4.42}$$

If equality holds at optimality, then the above relations are satisfied and the relaxation is regarded as exact. To further strengthen the proposed relaxation, we incorporate the Reformulation-Linearization Technique (RLT) technique [43]. Linear inequalities (4.40b) – (4.40e) are derived from (2.6). Lastly, inequalities (4.40g) – (4.40i) are immediate consequences of (4.5) and (2.6).

The variables that appear in (4.40) are tightly correlated and this is the primary motivation behind the proposed valid inequalities. In Section (4.5), we will demonstrate the

effect of these additional inequalities on the quality of relaxation and their ability to obtain feasible points.

4.4 FEASIBLE POINT RECOVERY

Let $\{x_{tg}^{\mathrm{rlx}}\}_{t\in\mathcal{T},\, g\in\mathcal{G}_t}$ denote the resulting schedule from a convex relaxation of SCUC. For large-scale problems, convex relaxations can fail to satisfy the integrality constraint (4.5). In this section, we propose a heuristic to infer a feasible point $\{\hat{x}_{tg} \in \{0,1\}\}_{t\in\mathcal{T},\, g\in\mathcal{G}_t}$. To this end, the main challenge is to ensure that the minimum up and minimum down constraints (2.7a) and (2.7b) are satisfied, which is not possible by simply rounding x_{tg}^{rlx} values. To tackle this issue we adopt the following procedure.

Feasible Point Recovery:

1) For every $t \in \mathcal{T}$ and $g \in \mathcal{G}_t$ do $x_{tg}^{\mathrm{rnd}} \leftarrow \mathrm{round}\{0.4 + x_{tg}^{\mathrm{rlx}}\}$.

2) For every $g \in \cup_{t\in\mathcal{T}}\mathcal{G}_t$,

(a) Solve the following linear program

$$\text{minimize} \quad \sum_{t\in\mathcal{T}} |x_{tg} - x_{tg}^{\mathrm{rnd}}| \tag{4.43a}$$

$$\text{subject to} \quad x_{tg} = 0 \quad \text{if} \quad g \notin \mathcal{G}_t \tag{4.43b}$$

$$0 \le x_{tg} \le 1 \quad \text{if} \quad g \in \mathcal{G}_t \tag{4.43c}$$

$$x_{tg} \ge x_{\tau g} - x_{(\tau-1)g} \quad \forall t\in\mathcal{T},\ \forall \tau \in \{t - m_g^{\uparrow} + 1, \ldots, t\} \tag{4.43d}$$

$$1 - x_{tg} \ge x_{(\tau-1)g} - x_{\tau g} \quad \forall t\in\mathcal{T},\ \forall \tau \in \{t - m_g^{\downarrow} + 1, \ldots, t\} \tag{4.43e}$$

and denote the resulting solution as $\{\hat{x}_{tg}\}_{t\in\mathcal{T}}$.

(b) For $t = 1, \ldots, |\mathcal{T}|$ do

$$a^{\uparrow}_{tg} \leftarrow \max\{\hat{x}_{\tau g} - \hat{x}_{(\tau-1)g} \mid \forall \tau \in \{t - m^{\uparrow}_{g} + 1, \ldots, t\}\}, \tag{4.44a}$$

$$a^{\downarrow}_{tg} \leftarrow \max\{\hat{x}_{(\tau-1)g} - \hat{x}_{\tau g} \mid \forall \tau \in \{t - m^{\downarrow}_{g} + 1, \ldots, t\}\}, \tag{4.44b}$$

$$\text{if} \quad a^{\uparrow}_{tg} = 0 \ \wedge \ a^{\downarrow}_{tg} = 0 \quad \text{then} \quad \hat{x}_{tg} \leftarrow x^{\mathrm{rnd}}_{tg}, \tag{4.44c}$$

$$\text{if} \quad a^{\uparrow}_{tg} = 0 \ \wedge \ a^{\downarrow}_{tg} = 1 \quad \text{then} \quad \hat{x}_{tg} \leftarrow 0, \tag{4.44d}$$

$$\text{if} \quad a^{\uparrow}_{tg} = 1 \ \wedge \ a^{\downarrow}_{tg} = 0 \quad \text{then} \quad \hat{x}_{tg} \leftarrow 1, \tag{4.44e}$$

$$\text{if} \quad a^{\uparrow}_{tg} = 1 \ \wedge \ a^{\downarrow}_{tg} = 1 \quad \text{then declare failure.} \tag{4.44f}$$

3) Declare $\{\hat{x}_{tg}\}_{t \in \mathcal{T},\, g \in \mathcal{G}_t}$ as the recovered schedule and solve the convex optimization

$$\text{minimize} \qquad \text{(2.1a)+(2.1b)+(2.1c)} \tag{4.45a}$$

$$\text{subject to} \qquad x_{tg} = \hat{x}_{tg} \qquad \forall t \in \mathcal{T}, \ \ \forall g \in \mathcal{G}_t \tag{4.45b}$$

$$\text{(2.6)} - \text{(4.27)} \qquad \forall t \in \mathcal{T}, \ \ \forall g \in \mathcal{G}_t \tag{4.45c}$$

$$\text{(2.10a)} \qquad \forall t \in \mathcal{T} \tag{4.45d}$$

to obtain a feasible point:

$$\{\hat{x}_{tg},\ \hat{p}^{\mathrm{ref}}_{tg},\ \hat{r}^{+}_{tg},\ \hat{r}^{-}_{tg},\ \hat{w}^{+}_{tg},\ \hat{w}^{-}_{tg},\ \hat{E}^{+}_{tg},\ \hat{E}^{-}_{tg} \in \mathbb{R}\}_{t \in \mathcal{T},\, g \in \mathcal{G}_t}$$

$$\{\hat{p}_{tgsc},\ \hat{p}^{+ESU}_{tgsc},\ \hat{p}^{-ESU}_{tgsc}\}_{t \in \mathcal{T},\, g \in \mathcal{G}_t,\, s \in \mathcal{S}_t,\, c \in \mathcal{C}_{ts}}.$$

In case of infeasibility, declare failure.

As we will demonstrate in Section (4.5), this heuristic is able to obtain good quality feasible points for challenging instances of SCUC. We use the following measure to evaluate the quality of the resulting feasible points:

$$\text{Optimality Gap } \% = 100 \times \frac{\hat{\sigma} - \sigma^{\text{rlx}}}{\hat{\sigma}} \tag{4.46}$$

where σ^{rlx} and $\hat{\sigma}$ are the optimal objective values for convex relaxation and the recovery problem (4.45), respectively.

4.5 EXPERIMENTS

The proposed SDP relaxation and recovery algorithm is tested on the MG scheduling problem under load demand uncertainty. Simulations are performed on a 64-bit computer with an Intel 3.0 GHz, 12-core CPU and 256 GB RAM using MATLAB 2019a. The MOSEK solver v8.0.0.60 [44] is used for convex optimization through CVX v2.1 [45, 46]. For comparison, CPLEX v12.9.0.0 [48] and GUROBI v9.0 are used for mixed-integer programming through MOST.

A modified IEEE 14-bus benchmark system is utilized to perform simulations. Parameters are obtained from the MATLAB MATPOWR package [52] with modifications made to DG cost, ESUs cost and load demand profiles. A single-line diagram of the benchmark system is depicted in Figure 4.2; it consists of 5 thermal DGs, 5 ESUs and load demand assigned to load buses in the network. The scheduling period is 1 second with the scheduling time interval of 200 milliseconds.

To demonstrate the effectiveness of our proposed methods, we generate random DG parameters as motivated by [95] in order to make problems feasible and sufficiently challenging. Table 4.1 shows a summary of DGs and ESUs parameters and costs. Additionally,

we generate load demand scenarios from a combination of the three load types discussed in Section 4.2, namely:

- Scenario #1: Group 1 (i.e. base load)
- Scenario #2: Group 1 & Group 2 (i.e. base + peak load)
- Scenario #3: Group 1, Group 2 & Group 3 (i.e. base + peak + transient load)

Scenarios are assigned initial probabilities

$$\Phi_1 = \begin{bmatrix} 0.76 & 0.17 & 0.07 \end{bmatrix}^\top \tag{4.47}$$

respectively. Additionally, for every $t \in \mathcal{T} \setminus \{1\}$ the transition probability matrix is set to

$$\Phi_t = \begin{bmatrix} 0.68 & 0.10 & 0.22 \\ 0.30 & 0.60 & 0.10 \\ 0.02 & 0.30 & 0.68 \end{bmatrix} \tag{4.48}$$

For simulating DG outage contingencies, 4 DGs are selected for outage contingencies each represented with probability of $1/60$. Base scenario conditional probabilities are selected as $\psi_{ts0} = 0.1/|\mathcal{C}|$ for every $s \in \mathcal{S}$. Additionally, for every $c \in \mathcal{C}$ post-contingency probabilities are given by:

$$\begin{bmatrix} \psi_{t1c} \\ \psi_{t2c} \\ \vdots \\ \psi_{t|\mathcal{S}|c} \end{bmatrix} = \frac{1}{|\mathcal{C}|} \times \Phi_t \begin{bmatrix} \psi_{(t-1)10} \\ \psi_{(t-1)20} \\ \vdots \\ \psi_{(t-1)|\mathcal{S}|0} \end{bmatrix} \tag{4.49}$$

Table 4.1: Generator Parameters

Unit	DG #1	DG #2	DG #3	DG #4	DG #5	ESUs
α_{tg}^{sqr} (\$/MW^{2}hr)	0.001	0.003	0.003	0.003	0.002	0
α_{tg}^{lin} (\$/MWhr)	21.504	13.482	27.830	10.047	25.977	0
ζ_{tg} (\$/hr)	246.809	394.788	600.495	724.182	164.901	20
$\zeta_{tg}^{\uparrow}$ (\$/hr)	8,435.1	7,205.7	4,894.3	4,486.9	4,574.3	0.001
$\zeta_{tg}^{\downarrow}$ (\$/hr)	345.08	506.807	508.617	754.102	735.865	0.001
μ_{tg}^{+}, μ_{tg}^{-} (\$/MWhr)	21.504	13.482	27.830	10.047	25.977	0
η_{tg}^{+}, η_{tg}^{-} (\$/MWhr)	4.301	2.697	5.566	2.009	5.195	0
β_{tg}^{+}, β_{tg}^{-} (\$/MWhr)	107.521	67.411	139.151	50.233	129.884	0
κ_g (\$/MW^{2}hr)	411.6e05	1,083.8e05	1,199.4e05	1,081.8e05	806.3e05	0
Pmax (MW)	166.2	70	50	50	50	10
Pmin (MW)	0	0	0	0	0	-10
$m_g^{\uparrow}$ (h)	3	5	1	3	5	1
$m_g^{\downarrow}$ (h)	3	4	1	3	7	1
Initial state (h)	2	4	-2	4	2	1

4.5.1 Evaluation of Lower Bound

Table 4.2 reports the performance of SDP relaxation compared to CPLEX and GUROBI solvers, perspective and LP relaxation methods. These numerical methods are compared on : i) convex lower bound (LB) on the optimal cost, ii) cost of the recovered feasible solution, iii) optimality gap and iv) computation time $t(s)$. Simulations are performed on 5 realizations of test system parameters. In each simulation, the solver is terminated after 3,600s and optimality gap computed using 4.46. In each individual realization, the numerical solver tries to determine optimal values of 1,500 binary decision variables and 1,035,632 continuous variables.

Table 4.2 shows that all three methods of relaxation, namely SDP relaxation, Perspective and LP relaxations obtain a lower bound to the globally optimal solution in 4 of the 5 experiments performed. In experiment 5, perspective relaxation fail to find a convex lower bound to the optimization problem where as both LP and SDP relaxation successfully find a convex lower bound and feasible solutions. As expected, average computation time is higher in the case of SDP relaxation (31m 15s) as compared to Perspective (8m 38s) and LP (9m 50s) relaxation. This is predictable as SDP relaxation method is a computationally expensive method of relaxation. The merit of applying SDP relaxation in this problem lies

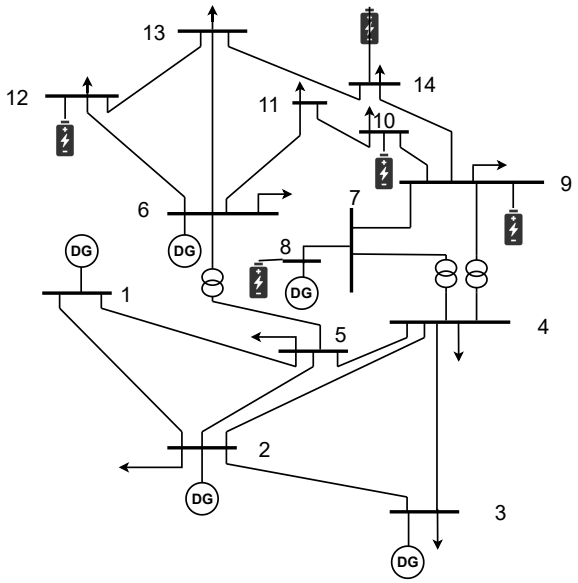

Figure 4.2: IEEE 14-bus Microgrid test system; showing ESUs placement in Experiment 5

Table 4.2: Comparative performance of SDP relaxation algorithm to off-the-shelf solvers and selected convex relaxations

Exp.	Test Case	CPLEX			GUROBI			SDP Relaxation				Perspective Relaxation				LP Relaxation			
		Feasible	GAP (%)	t(s)	Feasible	GAP (%)	t(s)	LB	Feasible	GAP (%)	t(s)	LB	Feasible	GAP (%)	t(s)	LB	Feasible	GAP (%)	t(s)
1	IEEE 14-bus	–	–	3,600†	–	–	3,600†	-1.667e+03	-1.667e+03	0.011	1,435	-1.667e+03	-1.667e+03	0.012	518	-1.667e+03	-1.667e+03	6.734e-05	715
2	IEEE 14-bus	–	–	3,600†	–	–	3,600†	-5.041e+03	-5.041e+03	0.002	2,034	-5.041e+03	-5.041e+03	0.003	513	-5.041e+03	-5.041e+03	9.580e-05	497
3	IEEE 14-bus	–	–	3,600†	–	–	3,600†	-5.907e+03	-5.907e+03	0.002	1,916	-5.908e+03	-5.908e+03	0.002	467	-5.908e+03	-5.908e+03	3.690e-05	432
4	IEEE 14-bus	–	–	3,600†	–	–	3,600†	-7.108e+03	-7.108e+03	0.002	2,176	-7.108e+03	-7.108e+03	0.002	652	-7.108e+03	-7.108e+03	4.454e-04	505
5	IEEE 14-bus	–	–	3,600†	–	–	3,600†	-1.057e+09	-1.057e+09	0.013	1,821	–	–	–	441	-1.057e+09	-1.057e+09	1.365e-04	574
Avg			–	–		–	–			0.006	1,876			0.005	518			1.614e-04	545
Max			–	–		–	–			0.011	2,176			0.012	652			4.45e-04	715

† Solvers are terminated within 3600 seconds.

in the fact that it can successfully find an optimal solution to the original MIP problem under uncertainty without a need to adopt scenario reduction methods when MIP solvers are used in the case of [86, 91, 92].

4.5.2 Utilizing Energy Storage Units to Compensate Variability in Load Profile

A major problem of MGs is inadequate reserve margins which adversely impacts its reliability. ESUs can be utilized to compensate for supply-demand mismatch which arises from the presence of highly variable load demand. In figure 4.3 we show benefits of ESUs to alleviate the burden of DGs in all three scenarios. We plot DG profile and ESU

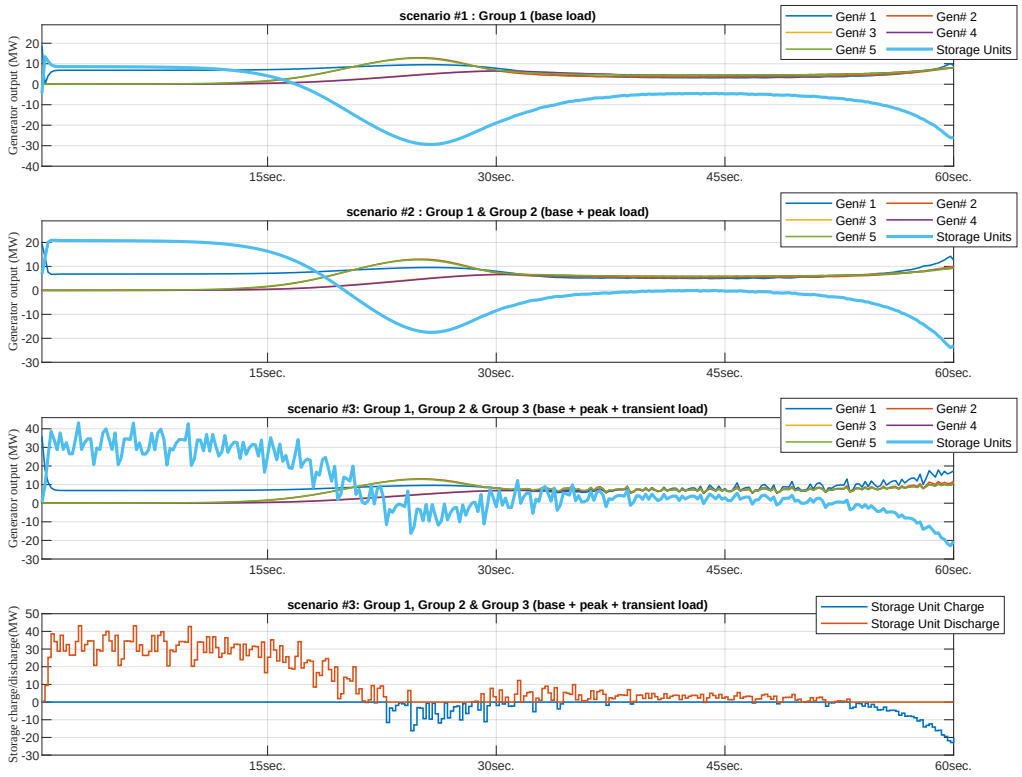

Figure 4.3: Impact of Energy Storage Units on load variability at 200ms time scales. First from top: DG and ESU power output in the presence of Group 1 (base loads). Second from top: DG and ESU power output in the presence of Group 1 & 2 (base + Peak loads). Third from top: DG and ESU power output in the presence of Group 1, 2 & 3 (base + peak + transient loads. Forth from top: ESU charge and discharge power output in scenario # 3.

charge and discharge levels over a period of 1 minute. It is observed that ESUs reduce the variability in Load profile in scenario #3. In scenario #3 when MG is subject to transient loads, ESUs alleviate the burden thereby increasing grid reliability.

Additionally, figure 4.3 presents the evolution of ESU charge and discharge levels over the time horizon. We observe that storage unit discharges energy to balance the high variability of transient load demand throughout the time horizon. This analysis can provide a guideline on determining the ESU size to achieve a desired supply-demand equilibrium across different load demand scenarios.

4.6 CONCLUSIONS

In this paper, we presented the Microgrid (MG) scheduling problem under load demand uncertainty. MGs by design have smaller network size and inadequate reserve margins as compared to the main grid. As a result, highly variable load like transient load demand can easily have adverse effects on reliability. To tackle this challenge in the MG scheduling problem, we proposed an SDP relaxation which is capable of finding feasible solutions within provable distance from global optimality. It is shown that the proposed SDP relaxation finds optimal solutions to the scheduling problem without need to adopt scenario reduction techniques when MIP solvers are utilized. Furthermore, we demonstrated that the problem of load variability can be greatly reduced with the help of Energy Storage Units (ESUs) when scheduled in tandem with Distributed Generators (DGs). The analysis performed can serve as a guide to MG operators in finding the approximate size of ESUs needed to achieve a desired load profile in a scheduling problem with the objective of minimizing operation cost.

CHAPTER 5

GENERAL CONCLUSIONS

5.1 Conclusions

In this article-based dissertation, an efficient computational optimization method is presented to deal with several complexities in power systems in 3 research papers. This research topic has been widely investigated for the last 60 years however scalable algorithms do not exist to the author's knowledge able to tackle problems of the scale presented in this dissertation at the time of writing. The algorithm developed in this research work has been tested on real-world grids with great results. Emphasizing its repeatability.

In Chapter 2, the proposed algorithm is used to tackle a stochastic security-constrained unit commitment problem which suffers from complexities posed by the presence of binary variables, probability distribution of uncertain parameters and security constraints. More than 12,000 binary variables are determined and almost 2 million continuous variables are deteremined through numerical experiments. In chapter 3, challenge of dealing with time-progressive contingencies such as hurricanes are tackled. As one of the major natural disasters that influence U.S. every year, the modeling and prediction of hurricane based on climatology and meteorology are critical and fundamental. For example, in 2017, Hurricane Irma and Maria stroke Puerto Rico as Category 5 storm, and caused prolonged yet wide-spread damage to Puerto Rico's electrical infrastructure. The experiment results indicate that this approach generates optimal results.

In Chapter 4, microgrid scheduling is explored in the presence of uncertainty in transient load demand. Through experiments, we demonstrate that Energy Storage Units have the potential to enhance MG reliability even in the presence of highly variable transient load demand.

5.2 Future Research Direction

The research work in this dissertation has many interesting directions for the future. Dimension of semidefinite matrices increases with the number of variables in the problem. As a result, SDP programming is computationally challenging to be solved with interior point solvers for higher order cones. One way of dealing with this is to decompose the larger semidefinite matrix into smaller cones. Thereby reducing the computational burdern of solving the large semidefinite matrix. Secondly, this idea opens up the possibility to utilize a parallelizable numerical algorithm that is capable of solving large-scale conic optimization problems on distributed platforms such as graphics processing unit (GPUs) with orders-of-magnitude time improvement.

Alternative Current (AC) network constraints introduce non-convexities into the problem formulation due to nonlinearities in voltage variable as a result system operators resort to the linear DC network constraints, also utilized in the papers presented here. Promising research indicates that nonlinearities in AC constraints can be tackled using SDP relaxation methods. An area for future research is to incorporate AC constraints into the stochastic SCUC formulation.

REFERENCES

[1] E. National Academies of Sciences and Medicine, *Analytic Research Foundations for the Next-Generation Electric Grid*. Washington, DC: The National Academies Press, 2016.

[2] R. Johnson, S. Oren, and A. Svoboda, "Equity and efficiency of unit commitment in competitive electricity markets," *Utilities Policy*, vol. 6, pp. 9–19, 03 1997.

[3] R. H. Kerr, J. L. Scheidt, A. J. Fontanna, and J. K. Wiley, "Unit commitment," *IEEE Transactions on Power Apparatus and Systems*, vol. PAS-85, no. 5, pp. 417–421, 1966.

[4] K. Hara, M. Kimura, and N. Honda, "A method for planning economic unit commitment and maintenance of thermal power systems," *IEEE Transactions on Power Apparatus and Systems*, vol. PAS-85, no. 5, pp. 427–436, 1966.

[5] R. C. Johnson, H. H. Happ, and W. J. Wright, "Large scale hydro-thermal unit commitment-method and results," *IEEE Transactions on Power Apparatus and Systems*, vol. PAS-90, no. 3, pp. 1373–1384, 1971.

[6] R. R. Shoults, S. K. Chang, S. Helmick, and W. M. Grady, "A practical approach to unit commitment, economic dispatch and savings allocation for multiple-area pool operation with import/export constraints," *IEEE Transactions on Power Apparatus and Systems*, vol. PAS-99, no. 2, pp. 625–635, 1980.

[7] F. N. Lee and Q. Feng, "Multi-area unit commitment," *IEEE Transactions on Power Systems*, vol. 7, no. 2, pp. 591–599, 1992.

[8] P. G. Lowery, "Generating unit commitment by dynamic programming," *IEEE Transactions on Power Apparatus and Systems*, vol. PAS-85, no. 5, pp. 422–426, 1966.

[9] J. D. Guy, "Security constrained unit commitment," *IEEE Transactions on Power Apparatus and Systems*, vol. PAS-90, no. 3, pp. 1385–1390, 1971.

[10] K. D. Le, J. T. Day, B. L. Cooper, and E. W. Gibbons, "A global optimization method for scheduling thermal generation, hydro generation, and economy purchases," *IEEE Power Engineering Review*, vol. PER-3, no. 7, pp. 25–26, 1983.

[11] M. L. Fisher, "Optimal solution of scheduling problems using lagrange multipliers: Part i," *Operations Research*, vol. 21, no. 5, pp. 1114–1127, 1973.

[12] D. Bertsekas, G. Lauer, N. Sandell, and T. Posbergh, "Optimal short-term scheduling of large-scale power systems," *IEEE Transactions on Automatic Control*, vol. 28, no. 1, pp. 1–11, 1983.

[13] J. A. Muckstadt and S. A. Koenig, "An application of lagrangian relaxation to scheduling in power-generation systems," *Operations Research*, vol. 25, no. 3, pp. 387–403, 1977.

[14] Yong Fu, M. Shahidehpour, and Zuyi Li, "AC contingency dispatch based on security-constrained unit commitment," *IEEE Transactions on Power Systems*, vol. 21, no. 2, pp. 897–908, 2006.

[15] ——, "Security-constrained unit commitment with ac constraints," *IEEE Transactions on Power Systems*, vol. 20, no. 3, pp. 1538–1550, 2005.

[16] X. Zhang, J. Zhao, and X. Chen, "A hybrid method of lagrangian relaxation and genetic algorithm for solving uc problem," in *2009 International Conference on Sustainable Power Generation and Supply*, April 2009, pp. 1–6.

[17] G. S. Lauer, N. R. Sandell, D. P. Bertsekas, and T. A. Posbergh, "Solution of large-scale optimal unit commitment problems," *IEEE Power Engineering Review*, vol. PER-2, no. 1, pp. 23–24, 1982.

[18] Y. Chen, A. Casto, F. Wang, Q. Wang, X. Wang, and J. Wan, "Improving large scale day-ahead security constrained unit commitment performance," *IEEE Transactions on Power Systems*, vol. 31, no. 6, pp. 4732–4743, 2016.

[19] G. B. Sheble and G. N. Fahd, "Unit commitment literature synopsis," *IEEE Transactions on Power Systems*, vol. 9, no. 1, pp. 128–135, 1994.

[20] A. S. Xavier, F. Qiu, F. Wang, and P. R. Thimmapuram, "Transmission constraint filtering in large-scale security-constrained unit commitment," *IEEE Transactions on Power Systems*, vol. 34, no. 3, pp. 2457–2460, 2019.

[21] Jiaying Shi and S. S. Oren, "Wind power integration through stochastic unit commitment with topology control recourse," in *2016 Power Systems Computation Conference (PSCC)*, 2016, pp. 1–7.

[22] G. Morales-España, J. M. Latorre, and A. Ramos, "Tight and compact milp formulation for the thermal unit commitment problem," *IEEE Transactions on Power Systems*, vol. 28, no. 4, pp. 4897–4908, 2013.

[23] E. R. Bixby, M. Fenelon, Z. Gu, E. Rothberg, and R. Wunderling, "Mip: Theory and practice — closing the gap," in *System Modelling and Optimization*, M. J. D. Powell and S. Scholtes, Eds. Boston, MA: Springer US, 2000, pp. 19–49.

[24] J. Ostrowski, M. F. Anjos, and A. Vannelli, "Tight mixed integer linear programming formulations for the unit commitment problem," *IEEE Transactions on Power Systems*, vol. 27, no. 1, pp. 39–46, 2012.

[25] J. Lee, J. Leung, and F. Margot, "Min-up/min-down polytopes," *Discrete Optimization*, vol. 1, pp. 77–85, 06 2004.

[26] P. Damci-kurt, S. Küçükyavuz, D. Rajan, and A. Atamtürk, "A polyhedral study of production ramping," *Mathematical Programming*, vol. 158, no. 1-2, pp. 175–205, 07 2016.

[27] S. R. Shukla, S. Paudyal, and S. Kamalasadan, "Tight conic formulation of unit commitment problem and comparison with minlp/milp formulations," in *2018 IEEE Power Energy Society General Meeting (PESGM)*, 2018, pp. 1–5.

[28] J. Alemany, L. Kasprzyk, and F. Magnago, "Effects of binary variables in mixed integer linear programming based unit commitment in large-scale electricity markets," *Electric Power Systems Research*, vol. In Press, 03 2018.

[29] A. Frangioni and C. Gentile, "A computational comparison of reformulations of the perspective relaxation: Socp vs. cutting planes," *Operations Research Letters*, vol. 37, no. 3, pp. 206–210, 2009.

[30] X. Bai and H. Wei, "Semi-definite programming-based method for security-constrained unit commitment with operational and optimal power flow constraints," *IET Generation, Transmission Distribution*, vol. 3, no. 2, pp. 182–197, 2009.

[31] S. Fattahi, M. Ashraphijuo, J. Lavaei, and A. Atamtürk, "Conic relaxations of the unit commitment problem," *Energy*, vol. 134, no. C, pp. 1079–1095, 2017.

[32] J. Liu, C. D. Laird, J. K. Scott, J. Watson, and A. Castillo, "Global solution strategies for the network-constrained unit commitment problem with ac transmission constraints," *IEEE Transactions on Power Systems*, vol. 34, no. 2, pp. 1139–1150, 2019.

[33] F. Zohrizadeh, M. Kheirandishfard, A. Nasir, and R. Madani, "Sequential relaxation of unit commitment with ac transmission constraints," in *2018 IEEE Conference on Decision and Control (CDC)*, 2018, pp. 2408–2413.

[34] C. E. Murillo-Sánchez, R. D. Zimmerman, C. L. Anderson, and R. J. Thomas, "Secure planning and operations of systems with stochastic sources, energy storage, and active demand," *IEEE Transactions on Smart Grid*, vol. 4, no. 4, pp. 2220–2229, Dec 2013.

[35] A. Majumdar, G. Hall, and A. Ahmadi, "A survey of recent scalability improvements for semidefinite programming with applications in machine learning, control, and robotics," *ArXiv*, 08 2019.

[36] D. K. Molzahn, F. Dörfler, H. Sandberg, S. H. Low, S. Chakrabarti, R. Baldick, and J. Lavaei, "A survey of distributed optimization and control algorithms for electric power systems," *IEEE Transactions on Smart Grid*, vol. 8, no. 6, pp. 2941–2962, Nov 2017.

[37] A. Ahmadi and A. Majumdar, "Dsos and sdsos optimization: More tractable alternatives to sum of squares and semidefinite optimization," *SIAM Journal on Applied Algebra and Geometry*, vol. 3, 06 2017.

[38] B. Kirby and M. Milligan, "A method and case study for estimating the ramping capability of a control area or balancing authority and implications for moderate or high wind penetration," *WINDPOWER 2005 Conference and Exhibition*, 01 2005.

[39] A. Frangioni and C. Gentile, "A computational comparison of reformulations of the perspective relaxation: Socp vs. cutting planes," *Oper. Res. Lett.*, vol. 37, no. 3, p. 206–210, May 2009.

[40] L. L. Garver, "Power generation scheduling by integer programming-development of theory," *Transactions of the American Institute of Electrical Engineers. Part III: Power Apparatus and Systems*, vol. 81, no. 3, pp. 730–734, 1962.

[41] J. A. Muckstadt and R. C. Wilson, "An application of mixed-integer programming duality to scheduling thermal generating systems," *IEEE Transactions on Power Apparatus and Systems*, vol. PAS-87, no. 12, pp. 1968–1978, 1968.

[42] A. I. Cohen and S. H. Wan, "A method for solving the fuel constrained unit commitment problem," *IEEE Transactions on Power Systems*, vol. 2, no. 3, pp. 608–614, 1987.

[43] H. D. Sherali and W. P. Adams, *Reformulation–Linearization Techniques for Discrete Optimization Problems*. New York, NY: Springer New York, 2013, pp. 2849–2896.

[44] MOSEK ApS, *The MOSEK optimization toolbox for MATLAB manual. Version 8.0.0.60*, 2016. [Online]. Available: https://docs.mosek.com/8.0/intro/index.html

[45] M. Grant and S. Boyd, "CVX: Matlab software for disciplined convex programming, version 2.1," http://cvxr.com/cvx, Mar. 2014.

[46] ——, "Graph implementations for nonsmooth convex programs," in *Recent Advances in Learning and Control*, ser. Lecture Notes in Control and Information Sciences, V. Blondel, S. Boyd, and H. Kimura, Eds. Springer-Verlag Limited, 2008, pp. 95–110, http://stanford.edu/~boyd/graph_dcp.html.

[47] R. D. Zimmerman, C. E. Murillo-Sanchez, and R. J. Thomas, "Matpower: Steady-state operations, planning, and analysis tools for power systems research and education," *IEEE Transactions on Power Systems*, vol. 26, no. 1, pp. 12–19, 2011.

[48] IBM, "Ilog cplex optimization studio v12.9.0," Mar. 2019.

[49] S. A. Kazarlis, A. G. Bakirtzis, and V. Petridis, "A genetic algorithm solution to the unit commitment problem," *IEEE Transactions on Power Systems*, vol. 11, no. 1, pp. 83–92, 1996.

[50] H. Kwon, J.-K. Park, D. Kim, J. Yi, and H. Park, "A flexible ramping capacity model for generation scheduling with high levels of wind energy penetration," *Energies*, vol. 9, p. 1040, 12 2016.

[51] Y.-H. Wan, "Wind power plant behaviors: Analyses of long-term wind power data," 01 2004.

[52] R. D. Zimmerman, C. E. Murillo-Sánchez, and R. J. Thomas, "Matpower: Steady-state operations, planning, and analysis tools for power systems research and education," *IEEE Transactions on Power Systems*, vol. 26, no. 1, pp. 12–19, 2011.

[53] U.S. NOAA National Centers for Environmental Information, "Billion-dollar weather and climate disasters: Overview"," https://www.ncdc.noaa.gov/billions/, accessed: 2021-07-22.

[54] National Infrastructure Advisory Council, "A framework for establishing critical infrastructure resilience goals," Tech. Rep., Oct. 2010.

[55] M. A. Elizondo, X. Fan, S. H. Davis, B. G. Vyakaranam, X. Ke, E. L. Barrett, S. F. Newman, P. D. Royer, P. V. Etingov, A. Tbaileh, H. Wang, U. Agrawal, W. Du, P. J. Weidert, D. A. Lewis, T. P. Franklin, N. A. Samaan, Y. V. Makarov, and J. E. Dagle, "Risk-based dynamic contingency analysis applied to puerto rico electric infrastructure," 5 2020. [Online]. Available: https://www.osti.gov/biblio/1771798

[56] S. H. Davis, M. A. Elizondo, X. Fan, S. F. Newman, E. L. Barrett, X. Ke, B. G. Vyakaranam, P. D. Royer, N. A. Samaan, and J. E. Dagle, "Data requirements for application of risk-based dynamic contingency analysis to evaluate hurricane impact to electrical infrastructure in puerto rico," 12 2020. [Online]. Available: https://www.osti.gov/biblio/1764377

[57] A. Arab, A. Khodaei, S. K. Khator, K. Ding, V. A. Emesih, and Z. Han, "Stochastic pre-hurricane restoration planning for electric power systems infrastructure," *IEEE Transactions on Smart Grid*, vol. 6, no. 2, pp. 1046–1054, 2015.

[58] X. Li, P. Balasubramanian, M. Sahraei-Ardakani, M. Abdi-Khorsand, K. W. Hedman, and R. Podmore, "Real-time contingency analysis with corrective transmission switching," *IEEE Transactions on Power Systems*, vol. 32, no. 4, pp. 2604–2617, 2017.

[59] M. Abdi-Khorsand, M. Sahraei-Ardakani, and Y. M. Al-Abdullah, "Corrective transmission switching for N-1-1 contingency analysis," *IEEE Transactions on Power Systems*, vol. 32, no. 2, pp. 1606–1615, 2017.

[60] M. Sahraei-Ardakani and G. Ou, "Day-ahead preventive scheduling of power systems during natuaral hazards via stochastic optimization," in *2017 IEEE Power Energy Society General Meeting*, 2017, pp. 1–5.

[61] Y. Sang, M. Sahraei-Ardakani, J. Xue, and G. Ou, "Comparing a new power system preventive operation method with a conventional industry practice during hurricanes," in *2019 North American Power Symposium (NAPS)*, 2019, pp. 1–6.

[62] L. Che, X. Liu, and Z. Li, "Preventive mitigation strategy for the hidden n-k line contingencies in power systems," *IEEE Transactions on Reliability*, vol. 67, no. 3, pp. 1060–1070, 2018.

[63] K. Lehmann, A. Grastien, and P. Van Hentenryck, "Ac-feasibility on tree networks is np-hard," *IEEE Transactions on Power Systems*, vol. 31, no. 1, pp. 798–801, 2016.

[64] J. Momoh, R. Koessler, M. Bond, B. Stott, D. Sun, A. Papalexopoulos, and P. Ristanovic, "Challenges to optimal power flow," *IEEE Transactions on Power Systems*, vol. 12, no. 1, pp. 444–455, 1997.

[65] A. S. Xavier, F. Qiu, F. Wang, and P. R. Thimmapuram, "Transmission constraint filtering in large-scale security-constrained unit commitment," *IEEE Transactions on Power Systems*, vol. 34, no. 3, pp. 2457–2460, 2019.

[66] R. Madani, M. Ashraphijuo, and J. Lavaei, "Promises of conic relaxation for contingency-constrained optimal power flow problem," *IEEE Transactions on Power Systems*, vol. 31, no. 2, pp. 1297–1307, 2016.

[67] P. Kaplunovich and K. Turitsyn, "Fast and reliable screening of N-2 contingencies," *IEEE Transactions on Power Systems*, vol. 31, no. 6, pp. 4243–4252, 2016.

[68] J. Lavaei and S. H. Low, "Zero duality gap in optimal power flow problem," *IEEE Transactions on Power Systems*, vol. 27, no. 1, pp. 92–107, 2012.

[69] R. Madani, S. Sojoudi, and J. Lavaei, "Convex relaxation for optimal power flow problem: Mesh networks," *IEEE Transactions on Power Systems*, vol. 30, no. 1, pp. 199–211, 2015.

[70] F. Zohrizadeh, M. Kheirandishfard, E. Q. Jnr, and R. Madani, "Penalized parabolic relaxation for optimal power flow problem," in *2018 IEEE Conference on Decision and Control (CDC)*, 2018, pp. 1616–1623.

[71] M. Zhao and M. Barati, "Low-order moment relaxation of acopf via algorithmic successive linear programming," in *2021 IEEE Texas Power and Energy Conference (TPEC)*, 2021, pp. 1–6.

[72] C. Coffrin, H. L. Hijazi, and P. Van Hentenryck, "Strengthening the sdp relaxation of ac power flows with convex envelopes, bound tightening, and valid inequalities," *IEEE Transactions on Power Systems*, vol. 32, no. 5, pp. 3549–3558, 2017.

[73] E. Quarm Jnr. and R. Madani, "Scalable security-constrained unit commitment under uncertainty via cone programming relaxation," *IEEE Transactions on Power Systems*, pp. 1–12, 2021.

[74] E3SM Project, "Energy Exascale Earth System Model (E3SM)," [Computer Software] https://e3sm.org/model/e3sm-model-description/, Apr. 2018.

[75] W. Bower, D. Ton, R. Guttromson, S. Glover, J. Stamp, D. Bhatnagar, and J. Reilly, "The advanced microgrid. integration and interoperability," 2014.

[76] S. S. Booth, J. Reilly, R. S. Butt, M. Wasco, and R. Monohan, "Microgrids for energy resilience: A guide to conceptual design and lessons from defense projects." [Online]. Available: https://www.osti.gov/biblio/1598145

[77] A. Khodaei, "Microgrid optimal scheduling with multi-period islanding constraints," *IEEE Transactions on Power Systems*, vol. 29, no. 3, pp. 1383–1392, 2014.

[78] Y. Zhang, N. Gatsis, and G. B. Giannakis, "Robust energy management for microgrids with high-penetration renewables," *IEEE Transactions on Sustainable Energy*, vol. 4, no. 4, pp. 944–953, 2013.

[79] A. G. Tsikalakis and N. D. Hatziargyriou, "Centralized control for optimizing microgrids operation," *IEEE Transactions on Energy Conversion*, vol. 23, no. 1, pp. 241–248, 2008.

[80] S. T. Cady, A. D. Domínguez-García, and C. N. Hadjicostis, "A distributed generation control architecture for islanded ac microgrids," *IEEE Transactions on Control Systems Technology*, vol. 23, no. 5, pp. 1717–1735, 2015.

[81] A. de Jesús Chica Leal, C. T. Rodríguez, and F. S. Piedrahita, "A proposal for microgrids control architecture as aggregator," in *2015 IEEE PES Innovative Smart Grid Technologies Latin America (ISGT LATAM)*, 2015, pp. 473–478.

[82] N. Troy, E. Denny, and M. O'Malley, "Base-load cycling on a system with significant wind penetration," *IEEE Transactions on Power Systems*, vol. 25, no. 2, pp. 1088–1097, 2010.

[83] M. Zachar and P. Daoutidis, "Microgrid/macrogrid energy exchange: A novel market structure and stochastic scheduling," *IEEE Transactions on Smart Grid*, vol. 8, no. 1, pp. 178–189, 2017.

[84] J. A. P. Lopes, C. L. Moreira, and A. G. Madureira, "Defining control strategies for microgrids islanded operation," *IEEE Transactions on Power Systems*, vol. 21, no. 2, pp. 916–924, 2006.

[85] W. Su, J. Wang, and J. Roh, "Stochastic energy scheduling in microgrids with intermittent renewable energy resources," *IEEE Transactions on Smart Grid*, vol. 5, no. 4, pp. 1876–1883, 2014.

[86] M. Alipour, B. Mohammadi-Ivatloo, and K. Zare, "Stochastic scheduling of renewable and chp-based microgrids," *IEEE Transactions on Industrial Informatics*, vol. 11, no. 5, pp. 1049–1058, 2015.

[87] B. Zhao, Y. Shi, X. Dong, W. Luan, and J. Bornemann, "Short-term operation scheduling in renewable-powered microgrids: A duality-based approach," *IEEE Transactions on Sustainable Energy*, vol. 5, no. 1, pp. 209–217, 2014.

[88] A. Khodaei, "Microgrid optimal scheduling with multi-period islanding constraints," *IEEE Transactions on Power Systems*, vol. 29, no. 3, pp. 1383–1392, 2014.

[89] M. Hemmati, B. Mohammadi-Ivatloo, M. Abapour, and A. Anvari-Moghaddam, "Optimal chance-constrained scheduling of reconfigurable microgrids considering islanding operation constraints," *IEEE Systems Journal*, vol. 14, no. 4, pp. 5340–5349, 2020.

[90] A. Parisio and L. Glielmo, "A mixed integer linear formulation for microgrid economic scheduling," in *2011 IEEE International Conference on Smart Grid Communications (SmartGridComm)*, 2011, pp. 505–510.

[91] A. Gholami, T. Shekari, F. Aminifar, and M. Shahidehpour, "Microgrid scheduling with uncertainty: The quest for resilience," *IEEE Transactions on Smart Grid*, vol. 7, no. 6, pp. 2849–2858, 2016.

[92] X. Wu, X. Wang, and C. Qu, "A hierarchical framework for generation scheduling of microgrids," *IEEE Transactions on Power Delivery*, vol. 29, no. 6, pp. 2448–2457, 2014.

[93] P. Kou, D. Liang, and L. Gao, "Stochastic energy scheduling in microgrids considering the uncertainties in both supply and demand," *IEEE Systems Journal*, vol. 12, no. 3, pp. 2589–2600, 2018.

[94] S. Ahn and S. Moon, "Economic scheduling of distributed generators in a microgrid considering various constraints," in *2009 IEEE Power Energy Society General Meeting*, 2009, pp. 1–6.

[95] E. Quarm Jnr. and R. Madani, "Scalable security-constrained unit commitment under uncertainty via cone programming relaxation," *IEEE Transactions on Power Systems*, pp. 1–1, 2021.

BIOGRAPHICAL STATEMENT

Edward Arthur Quarm Jnr. was born in Tema, Ghana, in 1989. He received his Bachelor of Science degree in Electrical and Electronic Engineering from Kwame Nkrumah University of Science and Technology (KNUST), Kumasi Ghana in 2013. He worked as a research assistant with KNUST for two years before obtaining a Master of Science degree in Systems Control from Universite Grenoble Alpes, Grenoble France in 2017. He joined the department of Electrical Engineering at The University of Texas at Arlington in 2017 where he served at a Graduate Teaching Assistant and Research Assistant from 2017 – 2021. His research was funded through the National Science Foundation under Grant ECCS-1809454. He is also a recipient of the STEM fellowship from 2017 – 2021. His research interests includes a broad area of control systems, machine learning, optimization and power systems.